INFORMATION TO USERS

This manuscript has been reproduced from the microfilm master. UMI films the text directly from the original or copy submitted. Thus, some thesis and dissertation copies are in typewriter face, while others may be from any type of computer printer.

The quality of this reproduction is dependent upon the quality of the copy submitted. Broken or indistinct print, colored or poor quality illustrations and photographs, print bleedthrough, substandard margins, and improper alignment can adversely affect reproduction.

In the unlikely event that the author did not send UMI a complete manuscript and there are missing pages, these will be noted. Also, if unauthorized copyright material had to be removed, a note will indicate the deletion.

Oversize materials (e.g., maps, drawings, charts) are reproduced by sectioning the original, beginning at the upper left-hand corner and continuing from left to right in equal sections with small overlaps. Each original is also photographed in one exposure and is included in reduced form at the back of the book.

Photographs included in the original manuscript have been reproduced xerographically in this copy. Higher quality 6" x 9" black and white photographic prints are available for any photographs or illustrations appearing in this copy for an additional charge. Contact UMI directly to order.

U·M·I

University Microfilms International
A Bell & Howell Information Company
300 North Zeeb Road, Ann Arbor, MI 48106-1346 USA
313/761-4700 800/521-0600

Order Number 1342996

Analysis of techniques to separate the ionizing-radiation-induced charge components in irradiated MOSFETs

Weber, William Martin, M.S.

The University of Arizona, 1990

Copyright ©1990 by Weber, William Martin. All rights reserved.

U·M·I
300 N. Zeeb Rd.
Ann Arbor, MI 48106

Analysis of Techniques to Separate the Ionizing-Radiation-Induced Charge Components in Irradiated MOSFETs

by

William Martin Weber

Copyright © William Martin Weber 1990

A Thesis Submitted to the Faculty of the
ELECTRICAL AND COMPUTER ENGINEERING DEPARTMENT
In Partial Fulfillment of the Requirements
For the Degree of
MASTER OF SCIENCE
WITH A MAJOR IN ELECTRICAL ENGINEERING
In the Graduate College
THE UNIVERSITY OF ARIZONA

1 9 9 0

STATEMENT BY AUTHOR

This thesis has been submitted in partial fulfillment of requirements for an advanced degree at the University of Arizona and is deposited in the University Library to be made available to borrowers under rules of the Library.

Brief quotations from this thesis are allowable without special permission, provided that accurate acknowledgement of source is made. Request for permission for extended quotation from or reproduction of this manuscript in whole or in part may be granted by the copyright holder.

SIGNED: W. Weben

APPROVAL BY THESIS DIRECTOR

This thesis has been approved on the date shown below:

R. D. Schrimpf — 26 November 1990

R. D. Schrimpf — Date

Professor of Electrical and Computer Engineering

DEDICATION

I would like to dedicate this thesis to my long suffering parents, Leo Enfield, the graduate students in the radiation lab at the U of Az, and all of the secretaries in the ECE department office. I believe that all of these people truly deserve a hardy round of '*thank you*' from me for their own special help in supporting my spirits through the two years I stayed at the U of Az.

ACKNOWLEDGEMENTS

I would, at this time, to thank those people who have made my thesis such a pleasure and joy to prepare. To Dr. Schrimpf, I award the Noble Prize for humanly dealing with my short comings. I thank Dr. Witulski for his unmitigated fairness in handling my thesis. I thank Dr. Galloway for his unwavering support of my research goals.

Table of Contents

LIST OF ILLUSTRATIONS 7

ABSTRACT 11

1. INTRODUCTION 12

1.1 Ionizing-Radiation-Induced Failures in Power MOSFETs 12

1.2 MOSFET Structure 12

1.2.1 The DMOS Structure 14

1.3 Ionizing-Radiation-Induced Charge 14

1.3.1 Oxide Trapped Charge 16

1.3.2 Interface State Production 16

1.3.3 Interface Trap Production Versus Oxide Charge 21

1.4 Transfer Characteristics 21

1.4.1 Mid-Gap Technique 22

1.4.2 Gate-Charge Curves for the MOSFET 23

1.5 Goals of This Thesis 23

2. THE MID-GAP METHOD 24

2.1 Mid-Gap Technique 24

2.1.1 Charge Separation 25

2.1.2 Above-Threshold I-V Relationship 25

2.1.2.1 Threshold Voltage 26

2.1.2.2 Voltage Shift Due to Trapped Charge at Threshold 26

2.1.3 Subthreshold 28

2.2 Theoretical Examination of the Mid-Gap Technique 30

2.2.1 Mobility Reduction 31

2.2.2 Analytical Example 34

2.2.3 Simulated Curves of the Subthreshold Region 38

2.3 Mid-Gap Error Due to Large Oxide Charge Build-Up 46

2.4 Data Extraction Using Mid-Gap Method 46

2.5 Summary 47

3. GATE-CHARGE TECHNIQUE 50

3.1 Gate-Charge Curve 50

3.2 Gate-Charge Technique 56

3.3 Gate-Charge Error Due to Large Oxide Charge Build-up 66

3.4 Data Extraction Using the Gate-Charge Method 67

4. COMPARISON BETWEEN MID-GAP AND GATE-CHARGE METHODS 70

4.1 Data from a Typical Transistor 70

4.2 Computer Simulation of Mid-Gap Method 72

4.3 Summary 76

5. SUMMARY AND CONCLUSION 78

5.1 Summary of Thesis 78

5.2 Conclusions 79

APPENDIX A - RADIATION EXPERIMENT 81

A.1 Device Types and Bias Conditions 81

A.2 Experimental Equipment for Mid-Gap Technique 82

A.3 Gate Charge Measurement 87

A.4 Gate Charge Curves 90

A.5 The Radiation Experiment 93

A.5.1 Radiation Source 93

A.5.2 Test Fixture 94

A.6 Summary 94

APPENDIX B - DATA FROM ALL TRANSISTORS 96

APPENDIX C - LISTING OF COMPUTER PROGRAM 100

LIST OF REFERENCES 113

List of Illustrations

Figure 1.1 - Diagram of an enhancement-mode n-channel MOSFET 13

Figure 1.2 - Diagram of an enhancement-mode n-channel DMOS transistor . . . 15

Figure 1.3 - Illustration of the electron-hole-pair production in a MOSFET . . . 17

Figure 1.4 - Diagram of the transition region from SiO_2 to Si 19

Figure 1.5 - Band diagram for the enhancement-mode n-channel MOSFET at inversion 20

Figure 2.1 - Plot of the subthreshold I-V region for an enhancement-mode n-channel MOSFET without interface traps generated from equation (2.8) . . . 32

Figure 2.2 - Plot of mobility reduction versus increase in interface-charge density . 35

Figure 2.3 - Diagram of simple differential interface-trap density distribution in energy 37

Figure 2.4 - Plot of the subthreshold I-V region for an enhancement-mode n-channel MOSFET with interface traps generated from equation (2.17) . . . 40

Figure 2.5 - Plot of the interface-charge underestimation found using the mid-gap method versus the density of interface-charge used in the subthreshold region simulation 42

Figure 2.6 - Effects of interface charge on the subthreshold equation separated into the effect of interface charge on V_{gs} and the effect of interface charge on the channel mobility 43

Figure 2.7 - Interface-charge underestimation using the mid-gap method versus the point where the interface-trap distribution changes from acceptor-like to donor-like 45

Figure 2.8 - Plot of threshold voltage shift resolved into interface and oxide charge components using the mid-gap method versus total dose of radiation IRH254 DMOS transistor 48

Figure 2.9 - Increase in interface charge found using the mid-gap method versus total dose of radiation from an IRH254 DMOS transistor 49

Figure 3.1 - Circuitry used to charge the gate during the gate-charge measurement . 51

Figure 3.2 - Gate-charge curve taken from a non-irradiated IRH254 DMOS transistor 52

Figure 3.3 - Equivalent circuit for the enhancement-mode n-channel MOSFET . . 53

Figure 3.4 - Physical layout of the enhancement-mode n-channel DMOS transistor including the capacitances C_{dg}, C_{gs}, and C_{it} 57

Figure 3.5 - Equivalent circuit for an irradiated MOSFET 59

Figure 3.6 - Idealized gate-charge curve illustrating the effects of interface traps . 61

Figure 3.7 - Differential interface trap distribution in energy 62

Figure 3.8 - Gate-charge curve taken from an IRH254 DMOS transistor before and after irradiation with the post radiation curve scaled 64

Figure 3.9 - Gate-charge curve taken from an IRH254 DMOS transistor before and after irradiation without the post radiation curve scaled 65

Figure 3.10 - Increase in interface charge found using the gate-charge method versus total dose of radiation from an IRH254 DMOS transistor 68

Figure 4.1 - Increase in interface charge as found using the mid-gap method versus increase in interface charge found using the gate-charge method for an IRH254 DMOS transistor 71

Figure 4.2 - Increase in interface charge found using the mid-gap method versus total dose from an IRH254 DMOS transistor 73

Figure 4.3 - Increase in interface charge found using the gate-charge method versus total dose from an IRH254 DMOS transistor 74

Figure 4.4 - Comparison of interface charge found using the mid-gap method to the interface charge found using the gate-charge method 75

Figure 4.5 - Plot of the ratio of the known interface charge density divided by the interface charge density found using the mid-gap method versus interface charge used in the simulation of the subthreshold region . . 77

Figure A.1 - Typical above-threshold I-V relationship taken from a transistor using an HP4145b parameter analyzer 83

Figure A.2 - Figure A.1 plotted as the square-root of the drain current versus gate voltage 84

Figure A.3 - Typical subthreshold I-V relationship taken from a transistor using an HP4145b parameter analyzer 86

Figure A.4 - Diagram of the experimental setup used to take the gate-charge curve 88

Figure A.5 - Diagram of the circuitry used to charge the gate of the DUT while regulating the drain current 89

Figure A.6 - Gate charge curve taken on an IRH254 before irradiation 91

Figure A.7 - Gate-charge curve taken from an IRH254 after irradiation 92

Figure A.8 - Diagram of the radiation test fixture 95

ABSTRACT

Power Metal Oxide Semiconductor Field-Effect Transistors (MOSFETs) are widely used in power supplies for spaceborne electronic systems. Spacecraft are routinely subjected to ionizing radiation. Ionizing-radiation-induced charges alter the operation of the MOSFET. The mid-gap technique allows separation of the parameter shifts into components due to oxide trapped charge and interface trapped charge. However, non-linearity in the subthreshold curve results in an approximately 20% underestimation of the interface component of the threshold shift. A new characterization technique is presented based on the relation between gate charge and gate-source voltage. The results obtained using the gate-charge method agree with theoretical calculations.

CHAPTER I
INTRODUCTION

1.1 Ionizing-Radiation-Induced Failures in Power MOSFETs

Power Metal Oxide Semiconductor Field-Effect Transistors (MOSFETs) are widely used in power supplies for spaceborne electronic systems. Spacecraft are routinely subjected to ionizing radiation. Ionizing-radiation produces charge in the gate dielectric of the MOSFET, which alters its operation [1- 4]. Techniques have been developed to study the production of charge in the MOSFET gate oxide by ionizing radiation [5]. This thesis outlines the current state of characterization techniques and it examines the errors associated with the most popular technique, the mid-gap method. This thesis presents a new characterization technique based on the relationship between gate charge and gate-source voltage.

1.2 MOSFET Structure

Figure 1.1 illustrates the physical layout of the enhancement-mode n-channel MOSFET. The gate potential controls the number of carriers in the channel region, which controls the conductivity between the source and the drain. The electrical current flows from the drain to the source along the Silicon/Silicon dioxide (Si/SiO_2) interface. The source and drain are heavily n-type doped. The body is lightly p-type doped. The gate material is typically polysilicon. A layer of silicon dioxide (SiO_2) insulates the body from the gate.

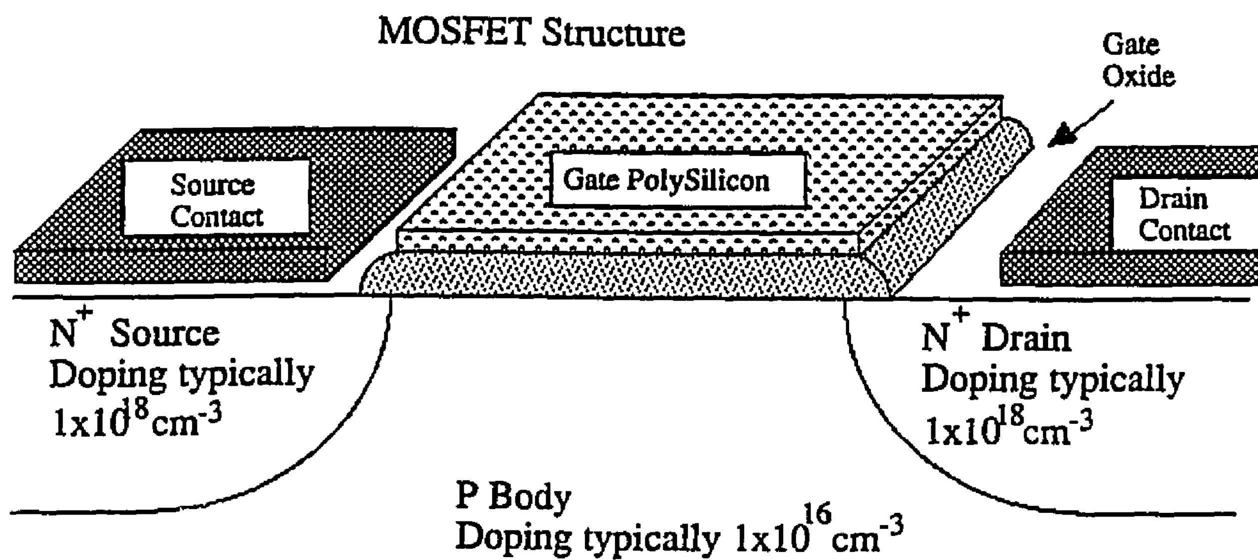

Figure 1.1 - Diagram of an enhancement-mode n-channel MOSFET.

1.2.1 The DMOS Structure

The Double-Diffused Metal-Oxide-Semiconductor (DMOS) transistor is a type of MOSFET. The DMOS transistor is frequently used in applications when the MOSFET is required to switch a large current or voltage [6]. Figure 1.2 illustrates the n-channel DMOS structure. The current flow in the DMOS transistor is controlled by the gate. The electrical current flows from the drain contact up to the Si/SiO_2 interface and then across the interface to the source. The source is doped heavily n-type. The drain is split into two regions. The drain region near the drain-to-body junction is lightly doped n-type. The drain region near the drain-to-metal contact is heavily n-type doped. The body is moderately doped p-type. The gate is polysilicon. An oxide insulates the gate from the substrate. Unlike the conventional MOSFET, the gate oxide and the gate polysilicon in the DMOS transistor extend over a significant portion of the drain region. Also, the body and source are electrically shorted together by the source metallization. The DMOS transistor functions on the same principles as the conventional MOSFET.

1.3 Ionizing-Radiation-Induced Charge

The study of ionizing-radiation-induced charge in MOSFETs has been an important field since the early 1960s [7]. The degradation of device performance due to ionizing radiation has been one of the limiting factors in using MOSFETs in a space radiation environment. Device degradation results from two types of radiation-induced charges: 1) oxide trapped charge and 2) interface trapped charge.

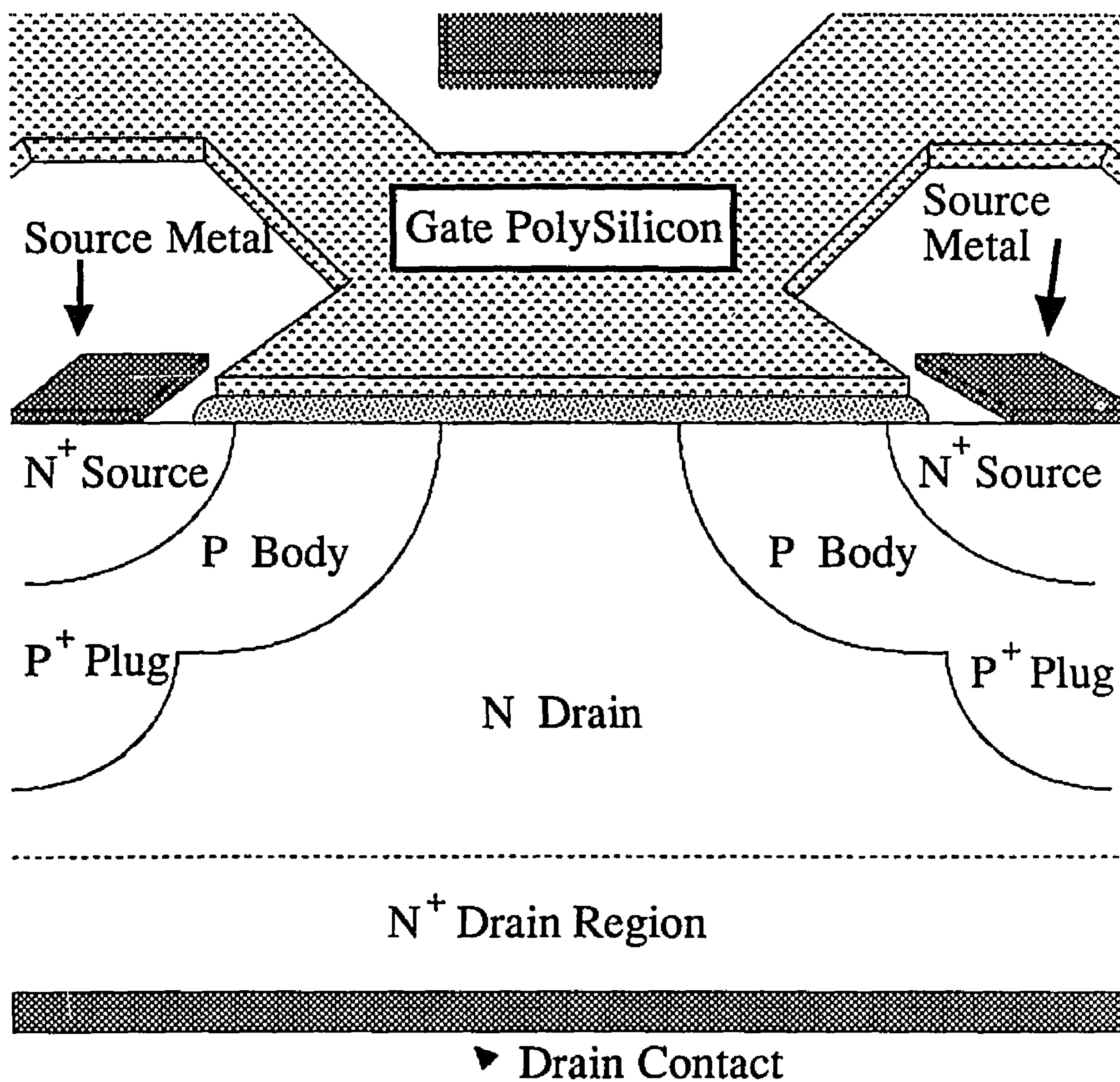

Body and N Epi Region Doping typically	$1\times10^{16}\ cm^{-3}$
Source, Plug and N Drain Region Doping typically	$1\times10^{18}\ cm^{-3}$

Figure 1.2 - Diagram of an enhancement-mode n-channel DMOS transistor.

1.3.1 Oxide Trapped Charge

Ionizing-radiation produces electron-hole pairs (EHPs) in any material it traverses. When photons strike the transistor, as illustrated in Fig. 1.3, EHPs are created [8]. The EHPs created in the bulk semiconductor material will easily recombine. In the gate dielectric (silicon dioxide, SiO_2) the EHPs are not as free to move. A fraction of the EHPs recombine. The electrons have a mobility in SiO_2 which is much higher than the mobility of the holes [9]. The remaining fraction of the electrons are swept out of the SiO_2, either by diffusion or an applied bias, leaving the holes behind. A fraction of the holes find sites which offer a lower eigen energy than any surrounding sites and become trapped. At this point, the charges are termed oxide trapped charge. The net oxide trapped charge is always positive.

1.3.2 Interface Trap Production

Interface traps are electrically active defects at the Si/SiO_2 interface which trap holes or electrons. It is hypothesized that these traps are formed from H^+ ions that are liberated from the oxide by the recombination of ionizing-radiation-induced EHPs [3].

During the first stage of trapped charge production, photons in the gate oxide produce EHPs. A fraction of the generated EHPs will recombine at recombination centers in the oxide. The energy lost during recombination (~9eV) is sufficient to liberate an H^+ ion contained in the defect center [3]. The H^+ ions which are liberated by the recombination travel by either diffusion or drift to the interface. Figure 1.4 illustrates the Si/SiO_2 interface [10]. The chemistry of the oxide changes greatly at the interface. The first few tens of angstroms of SiO_2 are very disordered, resulting in strained bonds between the silicon and oxygen. When the H^+ ions reach this transition region from SiO_2 to Si, they chemically react with the strained bonds of the SiO_x, producing charge trapping sites.

The chemistry of the H^+ ion reaction with the strained SiO_x bond will yield either a donor-like-trap or an acceptor-like-trap [11]. When the Fermi level rises above the energy level of the acceptor-like-trap, it will accept an electron from the silicon bulk material. When the Fermi level falls below the energy level of the donor-like-trap, it will donate an electron. Figure 1.5 defines the Fermi level and other energy levels in the MOS system. The acceptor-like-trap is neutral when the Fermi level is lower than its energy, and it becomes negatively charged when it accepts an electron. The donor-like-trap is neutral when the Fermi level is higher than its energy, and it becomes positively charged when it donates an electron.

When an interface trapping site is charged, it is referred to as an interface charge. Interface trapping sites may be neutral, positively charged, or negatively charged depending on their character and the position of the Fermi level.

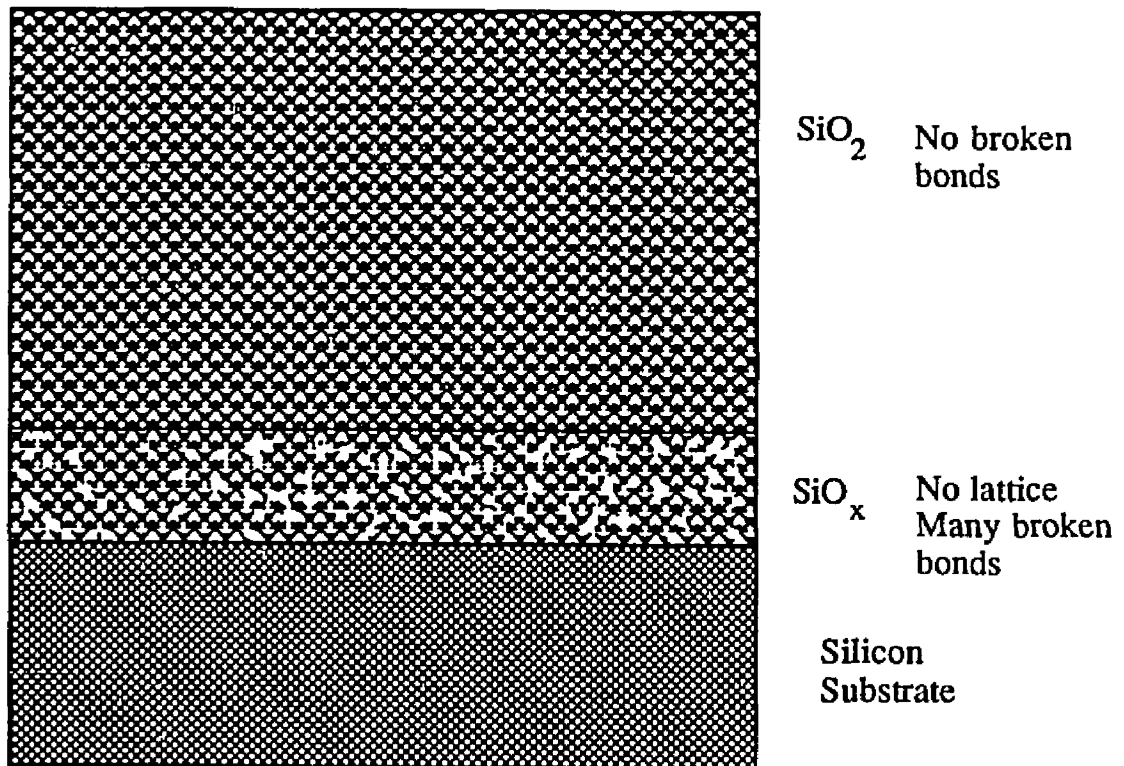

Figure 1.4 - Diagram of the transition region from SiO_2 to Si.

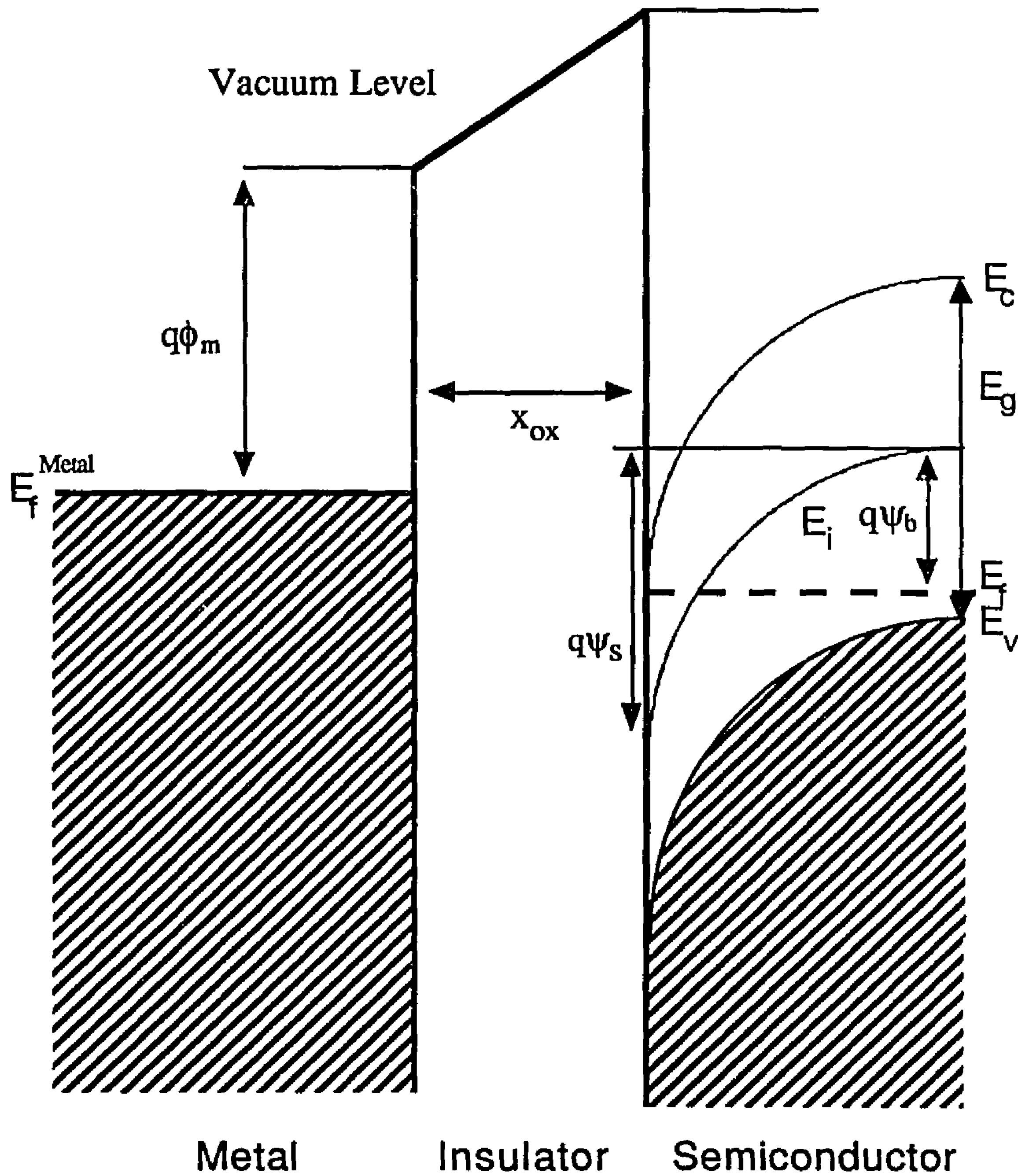

Figure 1.5 - Band diagram for the enhancement-mode n-channel MOSFET at inversion.

1.3.3 Interface Trap Production Versus Oxide Charge

Over the years of radiation experimentation done on MOSFETs, a trend in the relative magnitudes between oxide and interface charge has emerged. In commercial devices, the oxide charges typically far outnumber the interface traps. In radiation hardened devices, the interface and oxide charges are approximately equal. The interface traps rarely outnumber the oxide charges in MOSFETs. However, oxide trapped charge anneals with time, while interface traps may require significant time to form. Eventually interface charge may dominate. In n-channel devices, this phenomenon will be manifested as an increase in the threshold voltage. This is referred to as rebound, and it is particularly significant for devices irradiated at space dose rates.

1.4 Charge Separation

The mid-gap technique is a method for separating the effects of oxide and interface charge using the subthreshold and above-threshold I-V characteristics [5]. This technique is one of the most popular methods for charge separation. This thesis will propose a new method for separation, the gate-charge technique. Other methods for analyzing ionizing-radiation-induced charge exist, but are not applicable to commercially available DMOS devices. For example, the charge-pumping technique can find interface trap densities from transistors with a separate substrate connection [12].

1.4.1 Mid-Gap Technique

The mid-gap technique utilizes two I-V characteristics: the above-threshold I_d-versus-

V_{gs} and the subthreshold I_d-versus-V_{gs} characteristics.

1) Above-Threshold - The above threshold I_d-versus-V_{gs} transfer characteristic is used to find the increase in interface and oxide charge. When the channel region of the n-channel MOSFET is at threshold, all of the donor-like interface traps are neutral, and all of the acceptor-like traps are negatively charged. The oxide charge is always positive. The sum of oxide and interface charges is balanced by an equal amount of opposite-type charge to achieve charge neutrality. Changes in oxide and interface charge induce a variation of the charge density in the channel. This produces a shift in the threshold voltage. The mid-gap method uses the threshold-voltage shift to obtain the sum of the threshold voltage shift components due to ionizing-radiation-induced interface and oxide charge.

2) Subthreshold - When the surface potential is less than twice the bulk potential, the device is in the subthreshold region[13]. The mid-gap method assumes that all acceptor-like interface traps lie in energy above the middle of the silicon band-gap and all of the donor-like traps lie in energy below mid-gap. When the Fermi level is in the middle of the band-gap at the Si/SiO_2 interface, this assumption means that the interface traps should all be neutral. Thus any shift in the gate voltage at mid-gap must be due to oxide trapped charge. The mid-gap method is described in greater detail in Chapter Two.

1.4.2 Gate-Charge Curves for the MOSFET

A gate-charge curve is a plot of the gate-to-source voltage (V_{gs}) versus charge placed on the gate with a non-zero drain-to-source voltage (V_{ds}) applied. Circuit designers use these measurements to provide the necessary gate-drive requirements for power MOSFETs

[14]. After irradiation, the interface traps change the gate capacitance of the MOSFET. This new capacitance alters the relation between the gate voltage and gate charge. By noting the change in the gate capacitance, the total number of interface traps is found. The gate-charge method is described in greater detail in Chapter Three.

1.5 Goals of This Thesis

Changes observed in the electrical characteristics of a MOSFET are used to indicate the presence of ionizing-radiation-induced charge. The mid-gap method is used extensively to extract information on the production of ionizing-radiation-induced interface and oxide charge in the gate dielectric of the MOSFET. The mid-gap method assumes that the interface traps are neutral when the Fermi level is at mid-gap. The MOSFET subthreshold characteristics are used to find the gate voltage at mid-gap. This work illustrates how the interface traps alter the subthreshold characteristics. The alterations introduce errors in the mid-gap method.

A new charge-extraction technique is presented in this work which uses the gate-charge curve. This new method is tested against the mid-gap method. The results obtained from irradiated MOSFETs using both the mid-gap and gate-charge methods are correlated using a computer simulation of the mid-gap method. The computer simulation of the mid-gap method illustrates an approximately 20% error in the technique, which correlates to an approximately 20% difference in the results obtained from the mid-gap and gate-charge methods.

CHAPTER II
THE MID-GAP METHOD

2.1 Mid-Gap Technique

The mid-gap technique separates the effects of ionizing-radiation-induced interface and oxide charge using the subthreshold and above-threshold I_d-versus-V_{gs} relationships of an irradiated MOSFET [5]. The name derives from the assumption of the technique that the sites for trapping charge at the MOSFET Si/SiO_2 interface are not charged when the Fermi level is in the middle of the bulk silicon band-gap. The sites for trapping charge at the interface (hereafter termed interface traps) will be neutral at mid-gap if all the interface traps which lie in energy below mid-gap are donor-like and all of the traps above mid-gap are acceptor-like. A donor-like trap will donate an electron when the Fermi level falls below its energy level; an acceptor-like trap will accept an electron when the Fermi level rises above its energy level [11]. A donor-like trap becomes positively charged when it donates an electron and an acceptor-like trap becomes negatively charged when it accepts an electron [11]. Since interface traps at mid-gap are neutral, changes observed in the I-V characteristics at mid-gap are due to ionizing-radiation-induced oxide charge. In the n-channel MOSFET, the mid-gap technique probes the interface traps which lie in energy above mid-gap. In the following discussion, interface charge refers to interface traps which are charged when the MOSFET is at threshold.

Figure 1.5 illustrates the band-gap and its energy levels for the n-channel MOSFET. This work was restricted to n-channel MOSFETs, but it can be extended to the p-channel

MOSFET.

2.1.1 Charge Separation

The mid-gap technique utilizes two electrical characterization measurements: the subthreshold I_d-versus-V_{gs} relationship and the above-threshold I_d-versus-V_{gs} relationship. The above-threshold curve is used to find the total interface and oxide charge production due to ionizing radiation from the net threshold-voltage shift after irradiation. The subthreshold curve is used to find the oxide charge by analyzing the changes at mid-gap after irradiation.

2.1.2 Above-Threshold I-V Relationship

The threshold voltage is defined as the gate-to-source voltage when the channel minority carrier density is equal to the background doping density. The surface potential, ψ_s, is defined as

$$\psi_s = \frac{kT}{q}\ln\left(\frac{n_p}{n_i}\right) + \psi_b \qquad (2.1)$$

where k is the Boltzman constant, T is the temperature, q is the electronic charge, n_p is the minority charge carrier density at the interface, n_i is the intrinsic carrier density of silicon, and ψ_b is the bulk potential. The magnitude of ψ_s is the amount of the band-bending in Fig. 1.5. The bulk potential is defined as

$$\psi_b = \frac{kT}{q}\ln\left(\frac{N_a}{n_i}\right) \qquad (2.2)$$

where N_a is the doping density of the channel and ψ_b is the bulk potential. At threshold, the minority carrier density at the interface is equal to the majority carrier density in the bulk. The threshold of strong inversion is defined as when the surface potential equals the

twice the bulk potential[13],

$$\psi_s = \frac{2kT}{q} \ln\left(\frac{N_a}{n_i}\right). \tag{2.3}$$

The definitions of ψ_s and ψ_b are given in Fig. 1.5.

2.1.2.1 Threshold Voltage

The current-voltage relationship in the saturation region is given by

$$I_d = \frac{mZ}{L} \mu_n C'_{ox}(V_{gs} - V_{th})^2 \tag{2.4}$$

where C'_{ox} is gate oxide capacitance per unit area, Z is the width of the gate area, L is the channel length, V_{gs} is the gate potential, μ_n is the electron mobility in the channel, V_{th} is the threshold voltage, and m is a function of the doping density (typically $m = 1/2$) [15].

When $V_{gs}=V_{th}$, Eq. (2.4) predicts that the drain current I_d is zero. Equation (2.4) is not valid at and below threshold since the drain current is non-zero below threshold. Equation (2.4) can be used to find the threshold voltage of the MOSFET from the intersection of the $\sqrt{I_d}$ -versus-V_{gs} curve with the V_{gs} axis when the MOSFET is in saturation. The pre-radiation threshold voltage is found from the saturation curve of a MOSFET before it is subjected to radiation.

2.1.2.2 Voltage Shift Due to Trapped Charge at Threshold

When the n-channel MOSFET is at threshold, the Fermi level at the Si/SiO_2 interface is above the middle of the band-gap. Radiation produces interface and oxide charge in the

MOSFET. If the interface traps are segregated into acceptor-like traps above mid-gap and donor-like below, the interface charge at threshold will be due to negatively charged acceptor-like traps. The net oxide-trapped charge is always positive. If the oxide and interface charges are assumed to be near the Si/SiO_2 interface, then the potential drop across the oxide due to these charges is found from Gauss' law:

$$V_{drop} = \frac{Q_{tot}\,\varepsilon_{ox}\,A}{x_{ox}} \tag{2.5}$$

where Q_{tot} is the algebraic sum of the interface and oxide charge, A is the gate area, and x_{ox} is the oxide thickness.

When the I-V characteristics are measured after irradiation to find V_{th}, the voltage drop due to the oxide and interface charge adds to the gate voltage applied to the MOSFET. The additional V_{drop} will shift V_{th}. The total increase in interface and oxide charge per unit area is found from the shift in V_{th},

$$\Delta Q'_{tot} = \frac{\Delta V_{th}}{C'_{ox}} \tag{2.6}$$

where ΔV_{th} is the change in threshold voltage after irradiation and $\Delta Q'_{tot}$ is the total charge in the oxide and interface charge per unit area. The threshold voltage shift is related to the voltage shift due to oxide and interface charge by [5]

$$\Delta V_{th} = \Delta V_{ot} + \Delta V_{it} \tag{2.7}$$

where ΔV_{ot} is the oxide-charge component of the threshold shift and ΔV_{it} is the interface-charge component.

Equation (2.7) is only useful if ΔV_{ot} can be separated from ΔV_{it}. The subthreshold region is used to measure the shift in the mid-gap gate-to-source voltage due to ionizing radiation. Since the interface traps were assumed to be neutral at mid-gap, any shift in the

mid-gap voltage must be due to oxide charge.

2.1.3 Subthreshold

The subthreshold current-voltage relationship is given by [16]

$$I_d = \mu_n \left(\frac{Z}{L}\right) \frac{a\, C_{ox}'}{2\,\beta^2} \left(\frac{n_i}{N_a}\right)^2 \left(1 - e^{-\beta V_d}\right) \frac{e^{\beta \psi_s}}{\sqrt{\beta \psi_s}}, \tag{2.8}$$

where β is the reciprocal of the thermal voltage ($\frac{kT}{q}$), n_i is the intrinsic carrier concentration, N_a is the body doping level, V_d is the drain-to-source potential, ψ_s is the surface potential, and

$$a = \frac{2\, \varepsilon_s\, x_{ox}}{\varepsilon_i\, L_d} \tag{2.9}$$

where ε_s is the dielectric constant for silicon, ε_i is the dielectric constant for SiO_2, and L_d is the intrinsic Debye length[17]. The current-voltage relationship of Eq. (2.8) is approximately linear when plotted as the log of the drain current versus the linear gate voltage. The mid-gap technique requires knowledge of the MOSFET drain current and gate voltage when the surface potential is equal to the bulk potential (or equivalently when the Fermi level is at mid-gap). It is impossible to measure directly the drain current and gate voltage at mid-gap because the mid-gap current usually lies below the resolution of the current meters or is lower than the leakage currents of the device. Instead, the linear log(I_d)-versus-V_{gs} curve is extrapolated back to mid-gap. The current at the mid-gap condition is given by [5]

$$I_{mg} = \frac{G_m}{V_d} \frac{a}{2\, \beta^2} \frac{n_i^2}{N_a} \frac{e^{\beta\, \psi_b}}{\sqrt{\beta\, \psi_b}} \tag{2.10}$$

where G_m is the MOSFET gate transconductance. The transconductance relates the incremental increase in the drain current to the incremental increase in gate voltage and is

defined as

$$G_m = \frac{\partial I_d}{\partial V_{gs}} . \tag{2.11}$$

The gate transconductance is found from the slope of the saturation I-V characteristics of the device. Using the pre-radiation $\log(I_d)$-versus-V_{gs} curve, the gate voltage corresponding to mid-gap is found by extrapolating the curve back to the drain current at mid-gap.

After irradiation, the subthreshold relationship is changed due to oxide and interface charge. The gate voltage corresponding to mid-gap is found again by extrapolating the subthreshold curve back to the drain current at mid-gap. When the Fermi level is at mid-gap, the mid-gap method assumes that the interface traps are neutral. The shift in the gate voltage corresponding to mid-gap is due to oxide charge only, which is always positive. The oxide charge per unit area is found from Gauss' law

$$\Delta Q_{ot}^{'} = \frac{\Delta V_{mg}}{C_{ox}^{'}} \tag{2.12}$$

where ΔV_{mg} is the shift in mid-gap voltage and $\Delta Q_{ot}^{'}$ is the increase in oxide charge per unit area due to the radiation exposure. ΔV_{mg} is equal to the voltage shift due to oxide charge (ΔV_{ot}).

Since the voltage shift due to the increase in oxide charge is found from Eq. (2.12), the voltage shift due to the increase in interface charge at threshold is found by using Eq. (2.7).

The original derivation for the mid-gap method implicitly assumes that the subthreshold $\log(I_d)$-versus-V_{gs} remains linear after irradiation. After irradiation, the interface and

oxide charge shift the gate voltage. The charged interface traps also reduce the mobility [18]. Unlike the oxide charge, the interface trapped charge changes as a function of the gate-to-source voltage. Since the interface-charge density is a function of gate voltage, the post radiation log(I_d)-versus-V_{gs} curve is not linear.

2.2 Theoretical Examination of the Mid-Gap Technique

In this work, the effects of interface and oxide charge on the subthreshold current equation were examined analytically. The mid-gap technique was applied to curves produced analytically from Eq. (2.8) using known interface and oxide charge densities. The interface and oxide charge densities found from the mid-gap technique were compared to the known densities of charge used to generate the curves. To simplify the model, the oxide charge was set equal to zero since the oxide charge is constant for all V_{gs} values and thus only shifts the I_d-versus-V_{gs} curves by a constant amount.

The subthreshold region is described analytically by Eq. (2.8). The surface potential is related to the gate-to-source voltage by [19]

$$V_{gs} = \frac{1}{\beta}\left[\beta\psi_s + \hat{\psi}_s\frac{x_o'}{L_d}F(\psi_s,\psi_b)\right] - \phi_{ms} \quad (2.13)$$

where

$$F(\psi_s,\psi_b) \equiv \left[e^{\beta\psi_b}\left(e^{-\beta\psi_s} + \beta\psi_s - 1\right) + e^{-\beta\psi_b}\left(e^{\beta\psi_s} - \beta\psi_s - 1\right)\right]^{1/2}, \quad (2.14)$$

$$\hat{\psi}_s = \begin{Bmatrix} +1 & \text{if } \psi_s > 0 \\ -1 & \text{if } \psi_s < 0 \end{Bmatrix}, \quad (2.15)$$

$$x_o' = \frac{\varepsilon_s x_{ox}}{\varepsilon_i} \quad (2.16)$$

and ϕ_{ms} is the flat band voltage. In the subthreshold region, the second term in Eq. (2.13) is negligible. Thus in the subthreshold region, V_{gs} is directly proportional to ψ_s. If ψ_s is

replaced by V_{gs} in Eq. 2.8, the subthreshold equation becomes exponential in V_{gs} and the subthreshold log(I)-V curve is linear. Figure 2.1 shows a simulated subthreshold plot produced analytically from Eqs. (2.8) and (2.13). The subthreshold region deviates from purely exponential at lower V_{gs}. At lower gate-voltages, the square root in the denominator in eq. (2.8) dominates over the exponential.

The subthreshold current equation needs to be rewritten to accommodate interface and oxide charge after irradiation. The subthreshold equation now is

$$I_d = \mu_n(\psi_s)\left(\frac{Z}{L}\right)\frac{a\,C_{ox}'}{2\,\beta^2}\left(\frac{n_i}{N_a}\right)^2\left(1 - e^{-\beta V_d}\right)\frac{e^{\beta\psi_s}}{\sqrt{\beta\psi_s}} \qquad (2.17)$$

where $\mu_n(\psi_s)$ is the mobility as a function of the surface potential. The mobility changes as a function of the density of charged interface traps.

2.2.1 Mobility Reduction

The addition of charges in the oxide increases the scattering of the charge carriers in the channel due to the coulomb force. The coulomb force occurs between two charges. The coulomb force from the fixed interface and oxide charge to the charge carrier deflects the carrier from its course. The coulomb potential is given by

$$V_r = -\frac{q^2}{4\pi\varepsilon_o r} \qquad (2.18)$$

where r is the radial distance separating the two charges and ε_o is the dielectric constant of the material. Since the coulomb potential falls off as one over the radial distance, the charges which lie directly next to the channel region will contribute the greatest effect. The charged interface traps (which lie closer to the channel than the oxide charge) scatter the charge carriers in the channel [18]. The extra coulomb scattering due to the charged

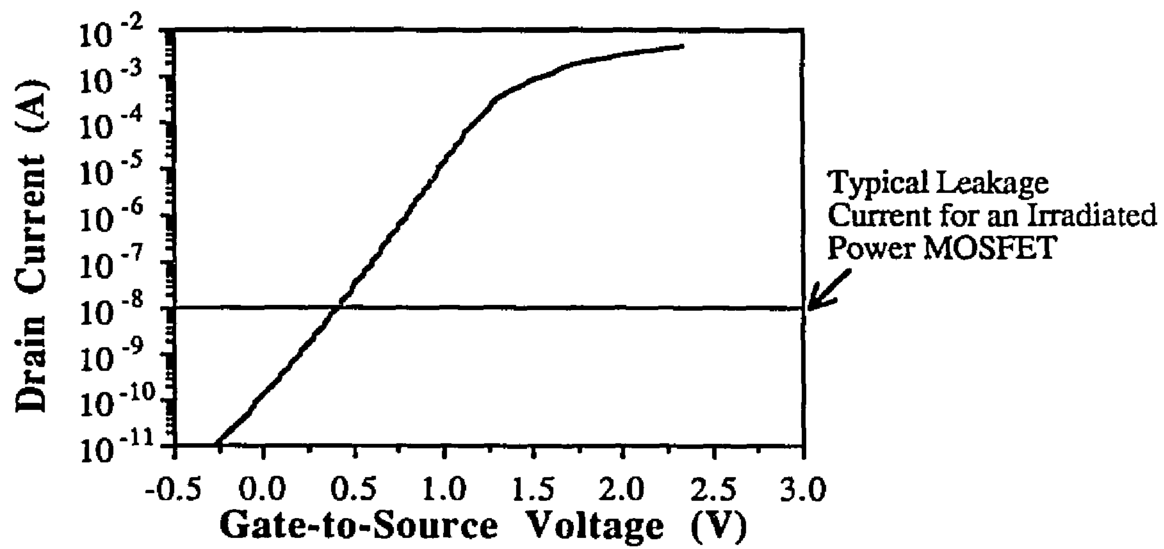

Figure 2.1 - Plot of the subthreshold I-V region for an enhancement-mode n-channel MOSFET without interface traps generated from equation (2.8).

interface traps serves to reduce the mobility of the charge carriers in the channel.

The radiation-induced reduction in mobility for the minority carriers is found from the MOSFET response to radiation in saturation. For a MOSFET in saturation, the current I_d^1 is given by

$$I_d^1 = \frac{mZ}{L} \mu_n C_{ox}' (V_{gs} - V_{th})^2 . \qquad (2.4)$$

where V_{gs} is the MOSFET gate voltage required to yield I_d^1 and V_{th} is the threshold voltage of the pre-radiation MOSFET. After irradiation, the same current I_d^1 is achieved at a different V_{gs} due to the threshold voltage shift and mobility reduction,

$$I_d^1 = \frac{mZ}{L} \mu_n' C_{ox}' (V_{gs}' - V_{th}')^2 \qquad (2.19)$$

where V_{gs}' is the new MOSFET gate voltage require to yield I_d^1, V_{th}' is the new threshold voltage and μ_n' is the reduced mobility. The ratio of the two mobilities is found from Eqs. (2.4) and (2.19)

$$\frac{\mu_n'}{\mu_n} = \frac{I_d^1 \frac{mZ}{L} C_{ox}' (V_{gs} - V_{th})^2}{I_d^1 \frac{mZ}{L} C_{ox}' (V_{gs}' - V_{th}')^2} \qquad (2.20)$$

or

$$\frac{\mu_n'}{\mu_n} = \frac{(V_{gs} - V_{th})^2}{(V_{gs}' - V_{th}')^2} . \qquad (2.21)$$

Figure 2.2 is a plot of the experimental mobility reduction found from Eq. (2.21) as a function of interface-charge density [20]. The experimental curve has been fit to the equation,

$$\mu_n^{eff} = \frac{\mu_o}{\alpha \, \Delta N_{it} + 1} \qquad (2.22)$$

where μ_n^{eff} is the effective mobility, α is an empirical constant, μ_o is the electron mobility before irradiation, and ΔN_{it} is the increase in the density of interface charge per unit area. α was found experimentally to be 8.6x10^{-12} cm^2 for the n-channel power MOSFETs used in the mobility reduction work performed by Schrimpf *et al* [20].

2.2.2 Analytical Example

In the subthreshold region, the interface traps will charge as a function of the position of the Fermi level, thus Eq. (2.22) becomes

$$\mu_n^{eff} = \frac{\mu_o}{\alpha\, \Delta\, N_{it}(\psi_s) + 1} \tag{2.23}$$

where $\Delta N_{it}(\psi_s)$ is the density of charged interface traps as a function of the surface potential. The surface potential is related to the gate-to-source voltage by

$$V_{gs} = \frac{1}{\beta}\left[\beta\psi_s + \hat{\psi}_s \frac{x_o'}{L_d} F\left(\psi_s, \psi_b\right)\right] + V_{it}(\psi_s) + V_{ot} - \phi_{ms}. \tag{2.24}$$

The term due to oxide charge is constant and only serves to shift the entire curve. For simplicity in the model, oxide charge was set equal to zero. The voltage shift due to interface traps in Eq. (2.24) is a function of the surface potential.

Application of the model begins by setting the surface potential. Taking a known interface-trap density distribution in energy, the number of charged interface traps is found using the surface potential. The acceptor-like traps which lie in energy below the Fermi level are charged. The effective mobility of the minority carriers in the channel is found from Eq. (2.23) using the calculated interface-charge density. The effective mobility and the known surface potential are used in Eq. (2.17) to find the drain current. The gate-to-source voltage is found using

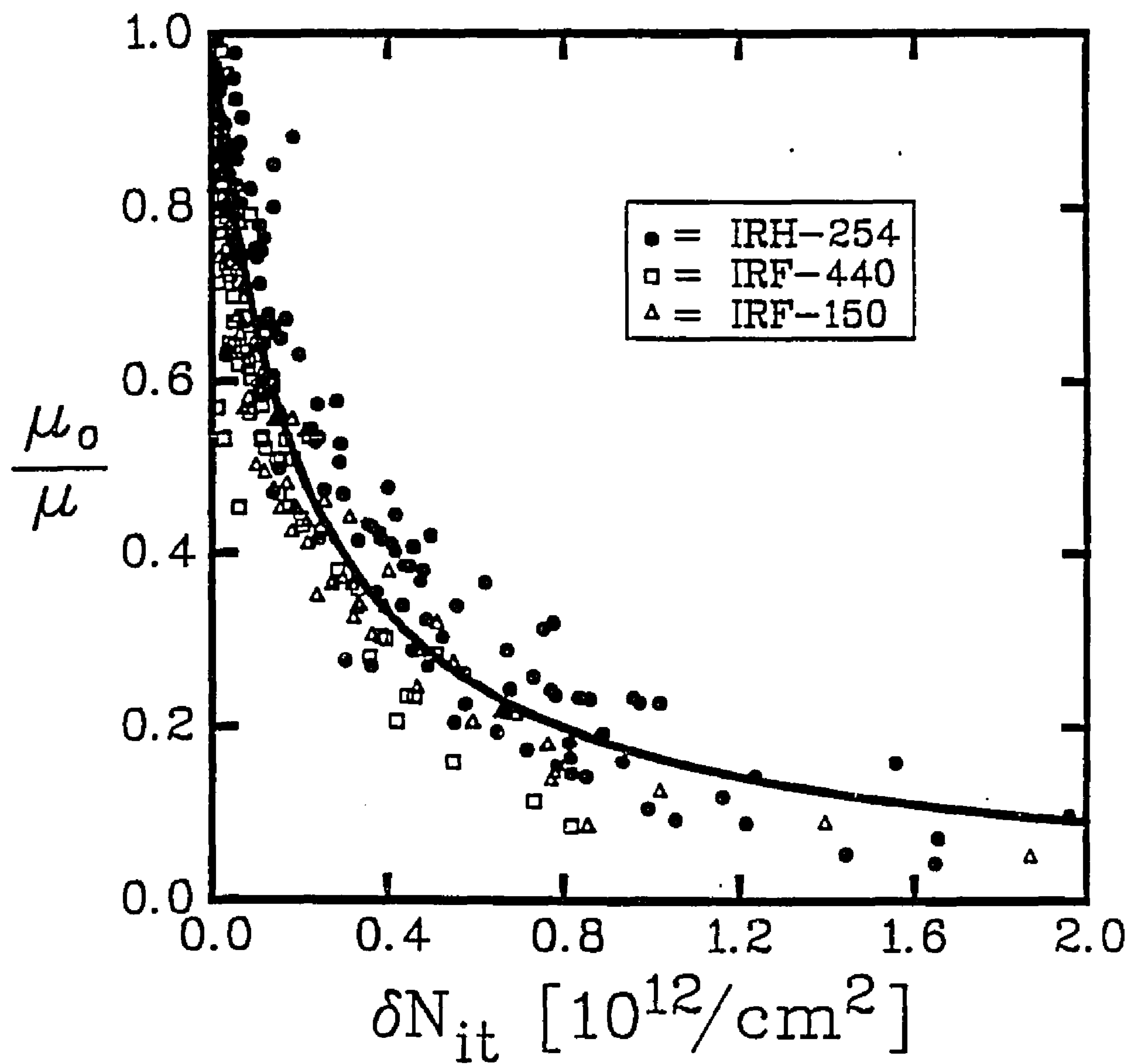

Figure 2.2 - Plot of mobility reduction versus increase in interface-charge density.

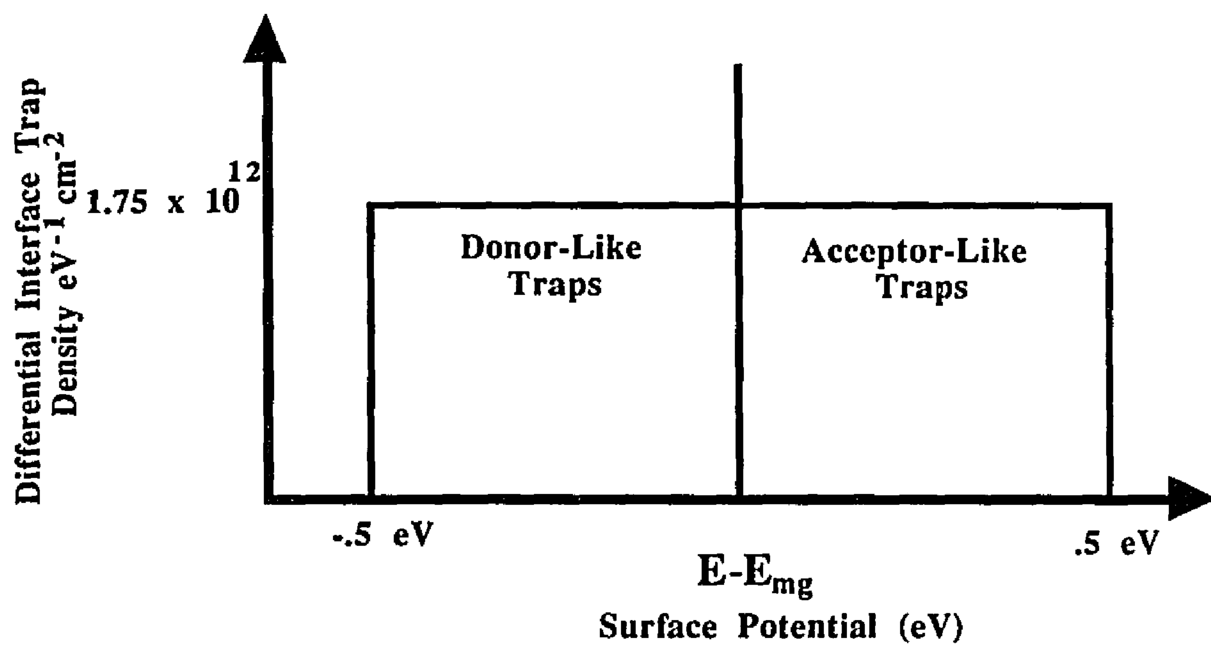

Figure 2.3 - Diagram of simple differential interface-trap density distribution in energy.

The gate-to-source voltage without interface charge is found by using Eqs. (2.18)-(2.22) with x_{ox} = 1000Å, ε_i equal to 3.9 (no units), ε_s equal to 11.9 (no units), ϕ_{ms} equal to 1.2 V, $\beta\psi_s$ equal to 21.2, $\beta\psi_b$ equal to 13.4, and L_d equal to $2.6\text{x}10^{-3}$ cm

$$x_o' = \frac{(11.9)(1000\text{x}10^{-8})}{3.9} = 3.05\text{x}10^{-5}\ \text{cm}\,.$$

$$F(\psi_s,\psi_b) = \left[e^{13.4}\left(e^{-21.2} + 21.2 - 1\right) + e^{-13.4}\left(e^{21.2} - 21.2 - 1\right)\right]^{1/2} = 3.7\text{x}10^{3}$$

$$V_{gs} = \frac{1}{38.6}\left[21.2 + \frac{3.05\text{x}10^{-5}}{2.3\text{x}10^{-3}}3.7\text{x}10^{3}\right] - 1.2\ V\ = 0.6\ V\,.$$

The interface trap charge degrades the mobility by 25% and shifts the gate-to-source voltage by qN_{it}/C_{ox}',

$$I_d^{nit} = 0.25\ I_d = 1.2\text{x}10^{-7}\ A$$

$$V_{gs}^{nit} = V_{gs} + \frac{\left(1.6\text{x}10^{-19}\right)\left(3.5\text{x}10^{11}\right)}{34\text{x}10^{-9}} = 2.3\ V\,.$$

2.2.3 Simulated Curves of the Subthreshold Region

The accuracy of the mid-gap method was studied using the analytical equations presented previously. The introduction of interface charge in the subthreshold equation affects the linearity of the log(I)-V characteristic. A computer simulation was used to produce the I-V curves from the subthreshold equation. The simulation produces an I-V curve for a MOSFET with a known interface-charge density. The mid-gap method was used on the simulated I-V curve with interface charge. The interface charge density found using the mid-gap method was compared to the interface-charge density which was used in the simulation. The values for the constants used in the computer simulation were identical to the values used in the analytical example in section 2.2.2.

Figure 2.1 illustrates a simulated subthreshold curve without interface states produced from Eqs. (2.8) and (2.13). The line in Fig. 2.1 represents the typical leakage current of an irradiated power MOSFET. Before irradiation, the leakage current of a power MOSFET is approximately 1×10^{-11} A. The leakage current can rise on a heavily irradiated MOSFET to approximately 1×10^{-6} A. The lower part of the subthreshold curve in Fig. 2.2 could not be seen on a real irradiated MOSFET I-V curve and the curve-fit to the I-V curve must be done on the upper part of Fig. 2.1. The current at mid-gap is 1×10^{-10} A. The mid-gap method finds the gate voltage at mid-gap by extrapolating the MOSFET subthreshold curve back to the mid-gap current. The straight-line fit to the simulated curve intersects the mid-gap current at a gate-to-source voltage of 0.1 V. The mid-gap voltage as given from Eq. (2.13) with $\psi_s = \psi_b$ is 0.1 V.

Figure 2.4 illustrates a simulated subthreshold curve with interface traps and no oxide charge. The curve fit intersects the mid-gap current at a gate-to-source voltage of -0.2 V. Since there was no oxide charge included, there should be no shift in V_{gs} at mid-gap. V_{gs} at mid-gap is given by Eq. (2.24) with $V_{ot} = 0$ and $\psi_s = \psi_b$ as 0.1 V. The mid-gap method attributes the shift in the mid-gap voltage to oxide charge. The voltage shift due to interface charge at threshold is found in the mid-gap method by subtracting the shift in the mid-gap gate-to-source voltage from the threshold voltage shift. Since the shift due to oxide charge at mid-gap is overestimated, the voltage shift due to interface charge is underestimated.

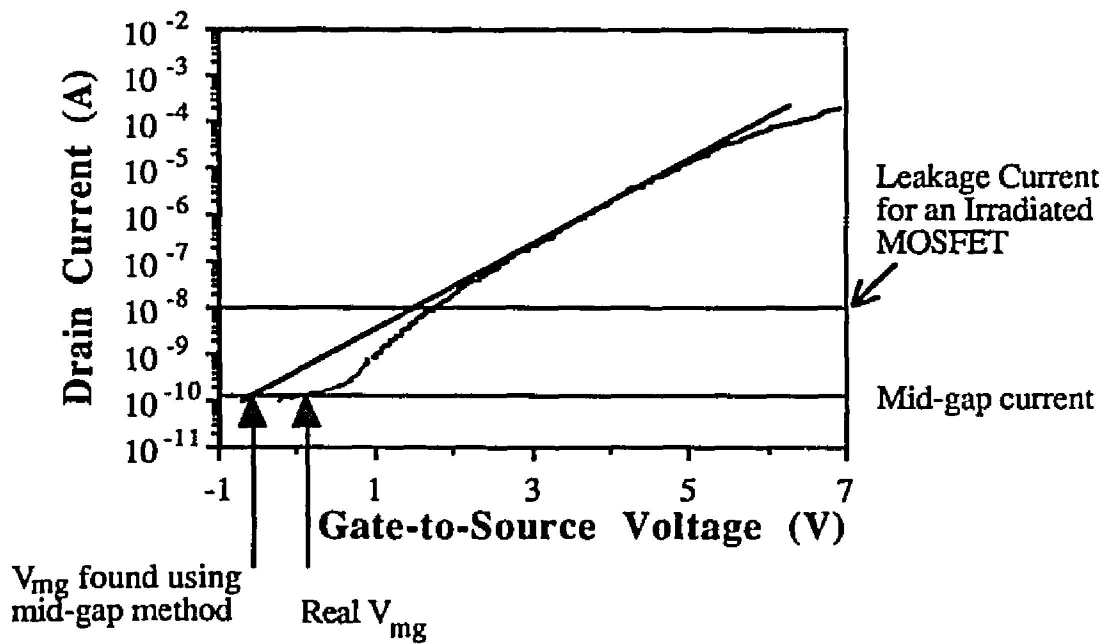

Figure 2.4 - Plot of the subthreshold I-V region for an enhancement-mode n-channel MOSFET with interface traps generated from equation (2.17).

Figure 2.5 is a plot of the interface-charge density used in the simulation divided by the interface-charge density found using the mid-gap method on the simulated subthreshold curves. This figure was generated with simulated subthreshold curves produced with increasing interface-charge density. The ratio rises to an approximately constant 1.23 (or 19% underestimation) for most interface charge densities. The error bars on Fig. 2.5 represent a ±5% error which is approximately the resolution limit of the 4145b parameter analyzer. The error in the mid-gap method is zero (or no underestimation) at zero interface-charge density. Since the error in the mid-gap method arises from the introduction of interface charge, with zero charge the underestimation should be zero.

The error in the mid-gap technique results from the distortion of the subthreshold curve by the effect of interface charge on the channel mobility and the surface potential. In Fig. 2.6, the subthreshold curve was simulated using no interface charge, using only the interface-charge effect on the mobility reduction, and again using only the interface-charge effect on V_{gs}. As Eq. (2.23) shows, the effect due to mobility reduction degrades the current as a function of the gate-to-source voltage. At mid-gap, the mobility reduction is zero and it increases toward threshold. The effect of the interface traps on V_{gs} is to stretch the current-voltage curve along the voltage axis. When an interface trap accepts an electron, the gate supplies an extra charge to balance the trapped charge. The extra charge on the gate increases the gate-to-source voltage without changing the surface potential. If the surface potential is not changed, the drain current will remain constant. Increasing the gate charge without increasing the drain current will stretch-out the I_d versus V_{gs} curve.

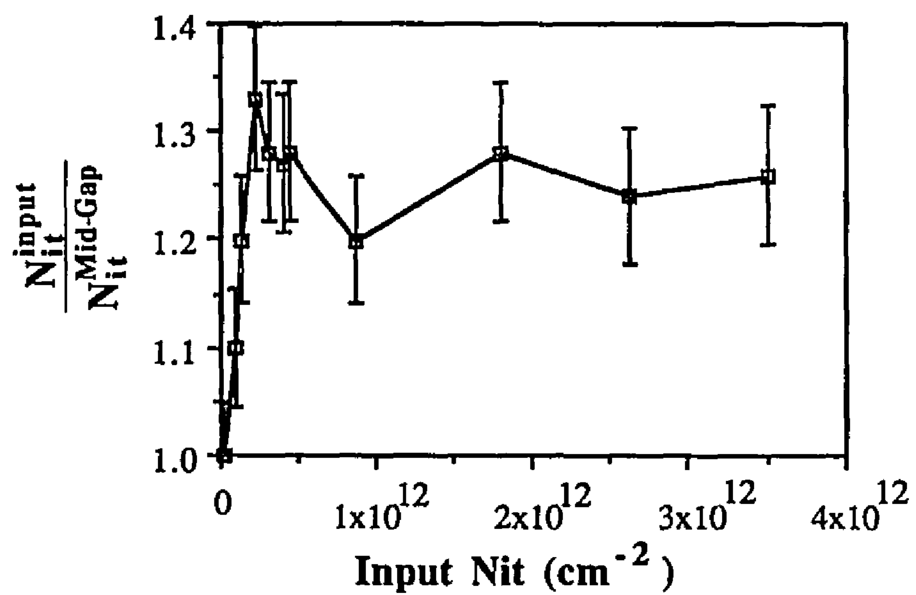

Figure 2.5 - Plot of the interface-charge underestimation found using the mid-gap method versus the density of interface-charge used in the subthreshold region simulation.

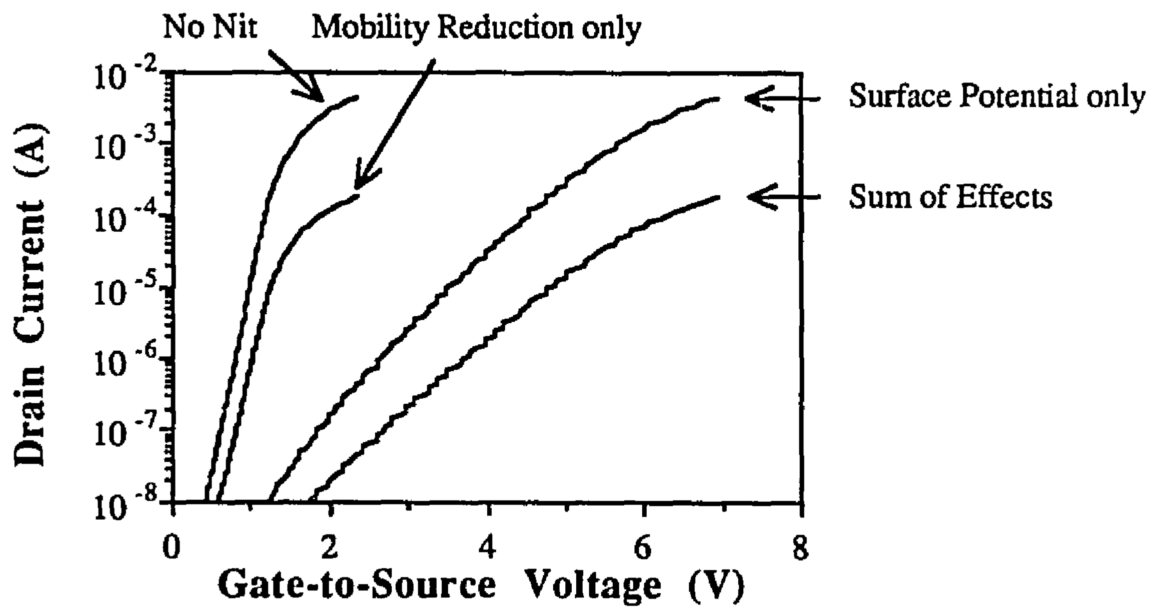

Figure 2.6 - Effects of interface charge on the subthreshold equation separated into the effect of interface charge on V_{gs} and the effect of interface charge on the channel mobility.

In Fig. 2.7, the ratio of interface-charge density used in the simulation divided by the interface-charge density found using the mid-gap method is plotted versus the point at which the interface trap distribution changes from donor-like to acceptor-like. Normally the interface traps are assumed to be segregated into all donor-like below mid-gap and all acceptor-like above mid-gap. In Fig. 2.7, the point where the interface-trap distribution changes from donor-like to acceptor-like was moved with respect to mid-gap, and then a subthreshold curve was generated. The error bars in Fig. 2.7 are ±5%. As the point for the change in the interface-trap distribution was lowered in the band-gap, the underestimation associated with the mid-gap method decreased. This was due to the interface traps being negatively charged by the time that the Fermi level reached mid-gap. By lowering the energy distribution of interface traps into the lower half of the band-gap, the interface traps at mid-gap are acceptor-like which are charged negatively. The mid-gap method associates the negative shift in V_{gs} at mid-gap after radiation to the build-up of positive oxide charge. Initially, the mid-gap method was shown to overestimate the oxide charge. By lowering the point for the change in the distribution, the interface traps at mid-gap are negatively charged, which subtracts from the overestimated positive oxide charge to yield a lower error. As the point of neutrality is lowered further, the underestimation in the interface component drops until the negative interface charge at mid-gap balances the overestimation of positive oxide charge. As the point is lowered further, the oxide charge becomes underestimated and the error swings in the other direction.

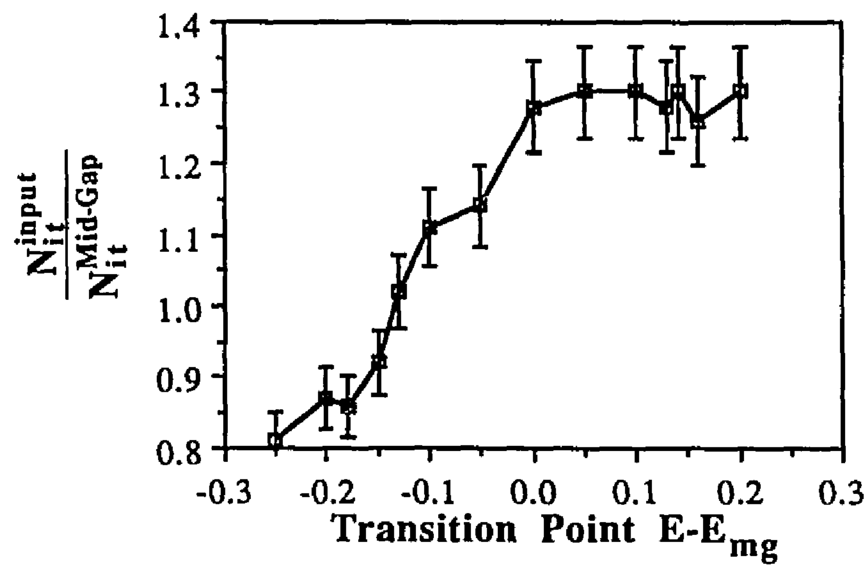

Figure 2.7 - Interface-charge underestimation using the mid-gap method versus the point where the interface-trap distribution changes from acceptor-like to donor-like.

2.3 Mid-Gap Error Due to Large Oxide Charge Build-Up

In many power MOSFETs, the amount of oxide charge is far greater than the amount of interface trapped charge. In these devices, the mid-gap method suffers from the effect of oxide charge swamping out the interface-charge contributions.

If the gate oxide of the transistor under study produces a larger oxide charge component than interface charge component, then the threshold shift will be primarily due to the oxide charge component. This occurs in many commercial devices. For a commercial power device after approximately 100 Krad(Si) of gamma radiation, the threshold shift might be ~ -9 V. If the shift due to oxide charge is calculated to be -10 V, the interface component should be 1 V. Assuming that the error in the measurement and analysis technique is approximately ±5%, then the oxide charge component could be anywhere between -10.5 and -9.5 V. The interface component could then be anywhere between 0.5 and 1.5 V. This range of interface trapped charge represents an error of ±50%. A 5% error in the oxide component of the threshold shift results in a 50% error in the interface component. This error is in addition to the errors described in section 2.2.

2.4 Data Extracted by Mid-Gap Method

Six transistors were irradiated following the procedure outlined in appendix A. The threshold voltage shift for one IRH254 is presented below and the data for the remaining five transistors are presented in appendix B. The radiation experiment was done to compare the mid-gap method to the gate-charge method which is presented in Chapter

Three. The difference in the interface component found using both methods is correlated in Chapter Four to the underestimation of the mid-gap method.

Figure 2.8 is a plot of the threshold voltage shift versus total dose for the IRH254 power MOSFET. The threshold voltage was resolved into the oxide and interface components by employing the mid-gap method as outlined in appendix A. Figure 2.9 is a plot of the increase in interface charge at threshold versus total dose for the IRH254. The interface charge was found from the interface component of the threshold shift by

$$\Delta Q_{nit} = \frac{\Delta V_{nit}}{C_{ox}} \qquad (2.25)$$

where C_{ox} is the oxide capacitance which for this device is found from the data sheets for the IRH254 to be 3400 pF.

2.5 Summary

The mid-gap technique is a widely used method for separating the effects of interface and oxide charge from the saturation and subthreshold I_d-versus-V_{gs} curves. The effect of interface charge on the subthreshold curve invalidates an implied assumption in the mid-gap technique. The assumption is that the subthreshold curve will remain linear after radiation when the log of the drain current is plotted versus the linear gate-to-source voltage.

A new technique is needed which will not be subject to the errors associated with the mid-gap technique. A new technique for charge separation which uses the gate-charge curve is presented in the next chapter.

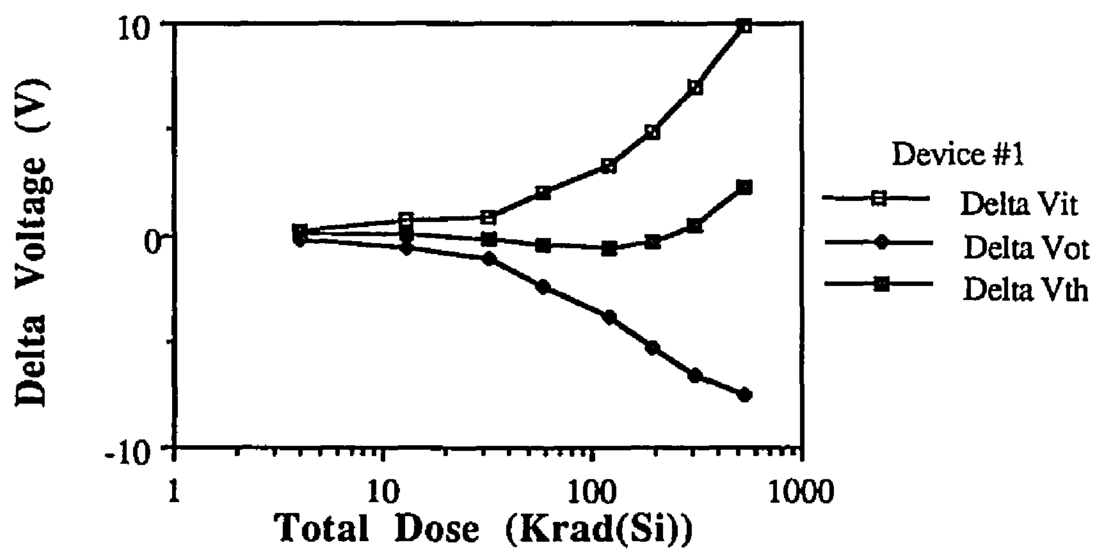

Figure 2.8 - Plot of threshold voltage shift resolved into interface and oxide charge components using the mid-gap method versus total dose of radiation IRH254 DMOS transistor.

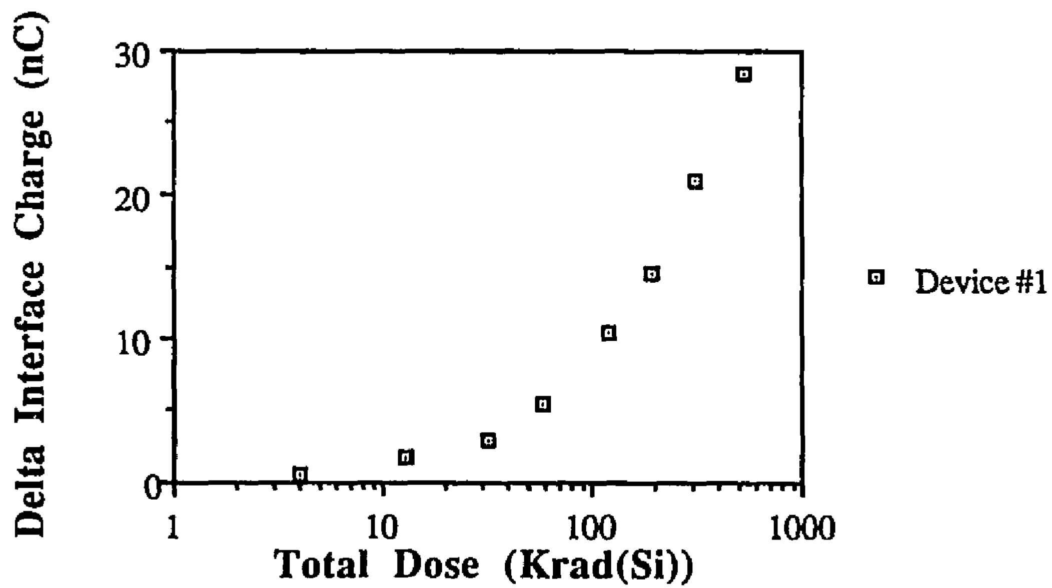

Figure 2.9 - Increase in interface charge found using the mid-gap method versus total dose of radiation from an IRH254 DMOS transistor.

CHAPTER III
GATE-CHARGE TECHNIQUE

A technique is presented that separates the effects of ionizing-radiation-induced interface and oxide charge using the gate-charge curve. The gate-charge curve uses the input capacitance of the gate to relate the gate voltage to the gate charge.

3.1 Gate-Charge Curve

A gate-charge curve is a plot of the gate-to-source voltage versus the gate charge as the gate is charged at a constant rate with V_{ds}>0 [14]. Figure 3.1 illustrates the circuitry used to charge the gate for the measurement. Figure 3.2 illustrates a typical gate-charge curve. Initially (when the gate charge=0), the input capacitance of the MOSFET gate is approximately equal to the gate-to-source capacitance (C_{gs}). In the DMOS structure, C_{gs} is the overlap capacitance formed when the source metallization overlaps the gate polysilicon (with an oxide in between). This overlap exists in most self-aligned DMOS processes [21].

Figure 3.3a illustrates the MOSFET equivalent circuit [21]. C_{dg} represents the drain output capacitance and is primarily controlled by the bias V_{ds}. The charge-carrier density in the channel controls the channel resistance R_{ds}. The charge on the MOSFET gate controls the charge-carrier density. The drain current I_o in Fig 3.3a is supplied by an external source. The current source $G_m V_{gs}$ represents the gate transconductance in the linear region of the MOSFET operation.

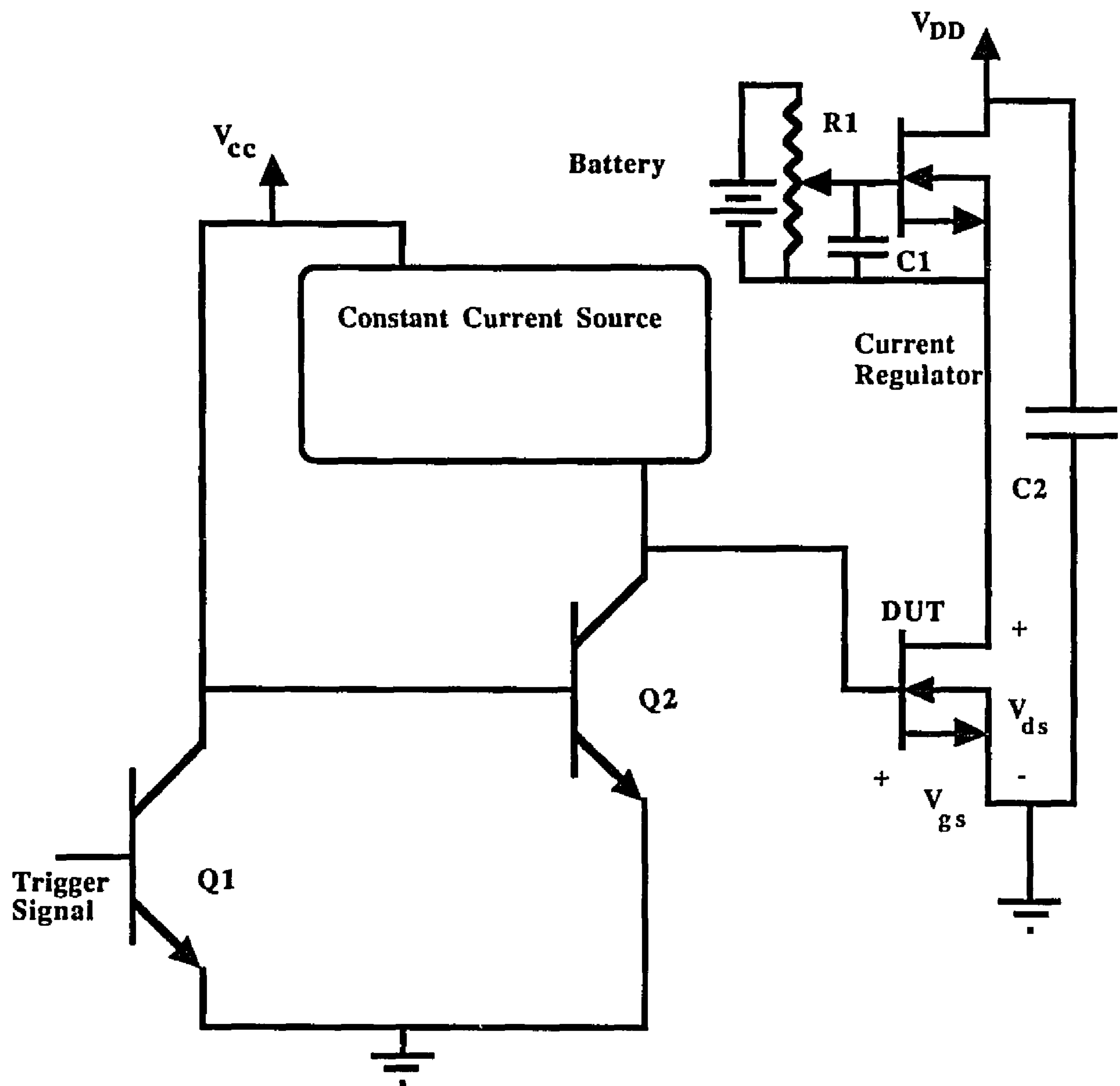

Figure 3.1 - Circuitry used to charge the gate during the gate-charge measurement.

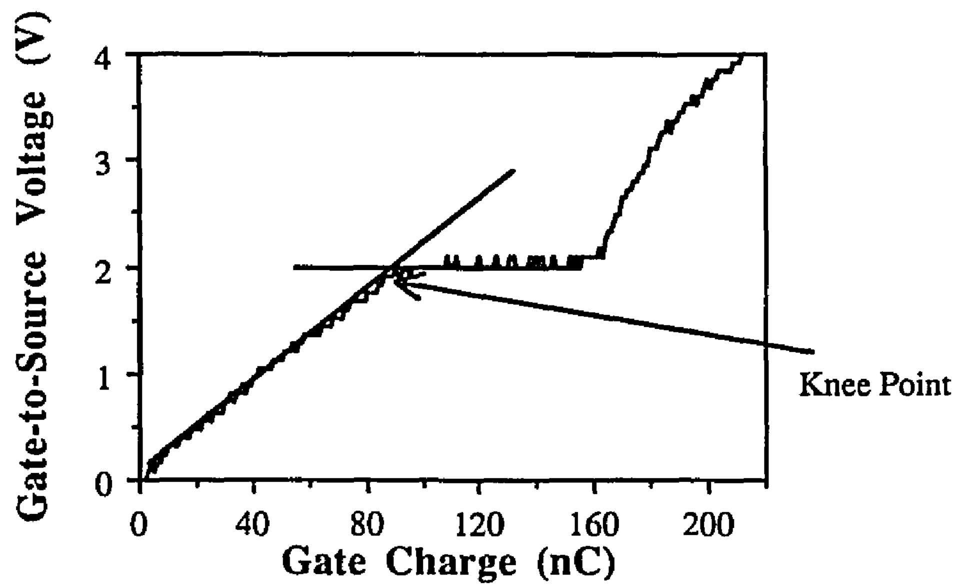

Figure 3.2a - Gate-charge curve taken from a non-irradiated IRH254 DMOS transistor.

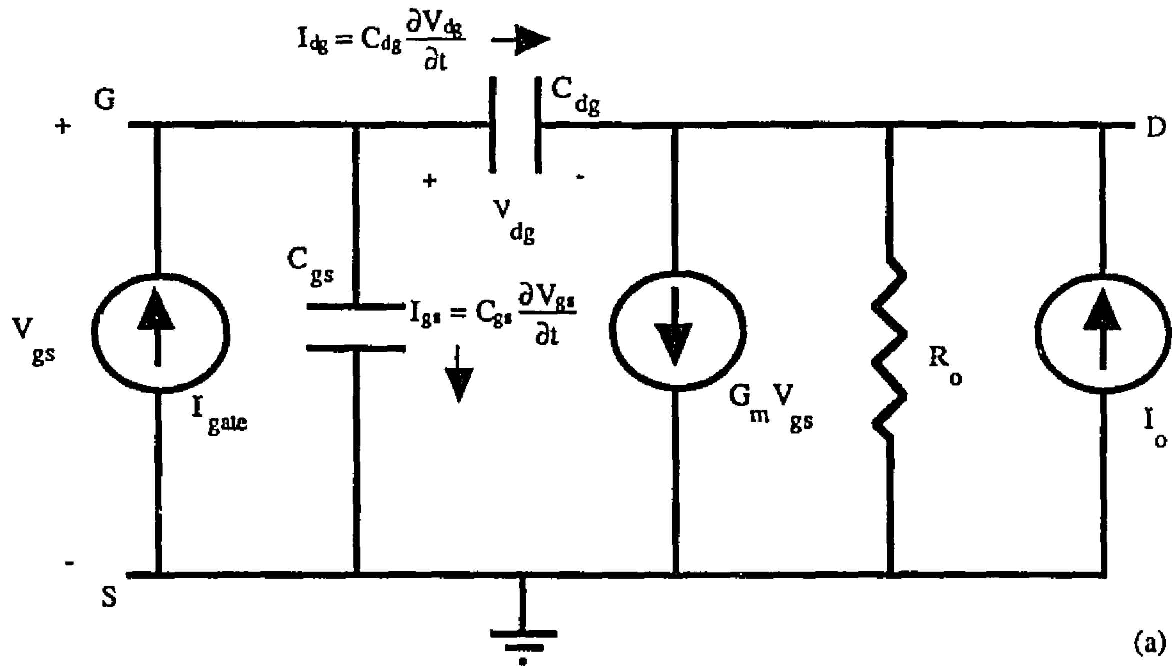

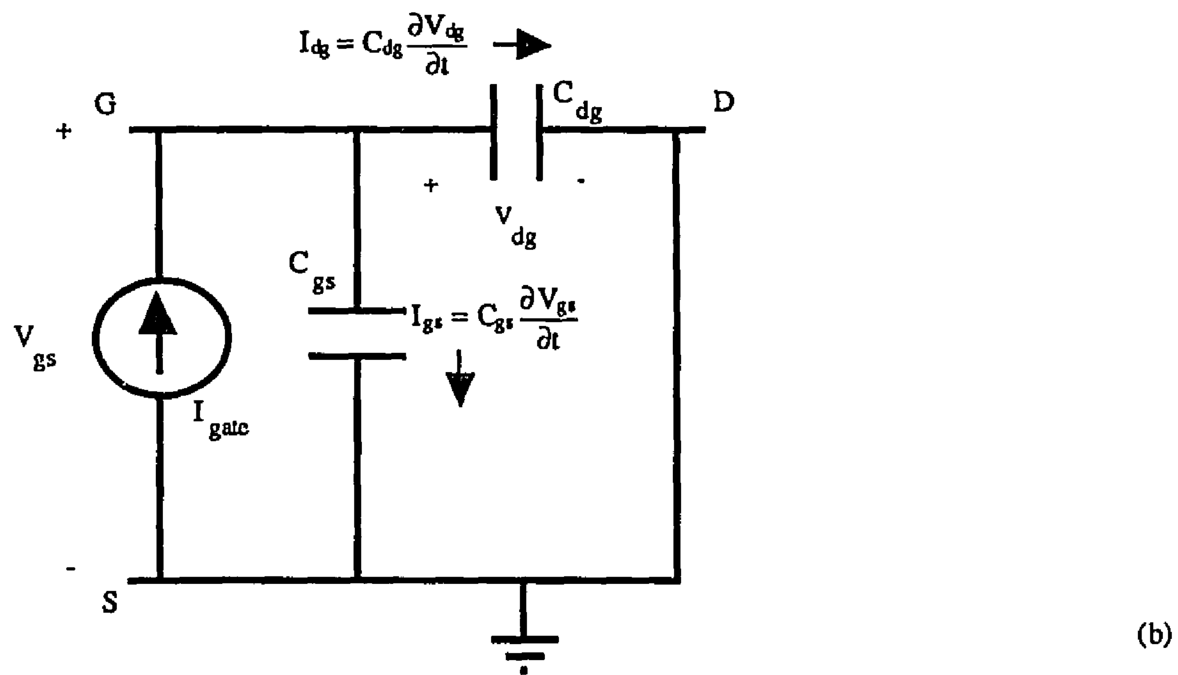

Figure 3.3a - Equivalent circuit for the enhancement-mode n-channel MOSFET.
Figure 3.3b - A.C. equivalent circuit for Fig. 3.3a.

where I_{gate} is the current into the gate. Placing positive charge on the n-channel MOSFET gate moves the channel region from accumulation to depletion to inversion. When the channel region enters inversion, the device is in saturation and the drain current (I_d) is related to V_{gs} by [15]

$$I_d = \frac{mZ}{L} \mu_n C'_{ox} (V_{gs} - V_{th})^2 \tag{3.6}$$

where C'_{ox} is the oxide capacitance per unit area, μ_n is the charge-carrier mobility in the channel, Z is the channel width, L is the channel length, m is a constant fixed by the channel doping density (typically m=1/2), and V_{th} is the threshold voltage. The limit on the current supply for I_d sets the maximum current which the channel region will conduct. The maximum current is labeled I_o^{on}. When the channel region inverts, the channel resistance will drop. As the channel resistance drops, V_{ds} decreases to $V_{ds}^{on} = I_o^{on} R_{ds}^{on}$ where R_{ds}^{on} is the channel on-resistance. The depletion region between the drain and the body (which V_{ds} supports) will also decrease. As the depletion region collapses, the space charge associated with the depletion region discharges into the channel. To achieve charge neutrality in the channel, extra charge must be placed on the gate to compensate for the depletion-region charge. This discharge of the depletion region produces the plateau region seen on the gate-charge curve in Fig. 3.2. The rate of discharge for V_{ds} is related to the gate charge by

$$\frac{\partial V_{ds}}{\partial t} = \frac{-I_{gate}}{C_{gd}} . \tag{3.7}$$

The MOSFET channel resistance R_{ds} in the plateau region drops from $\frac{V_{ds}}{I_o^{on}} = R_{ds}$ at the beginning of the plateau region to $\frac{V_{ds}^{on}}{I_o^{on}} = R_{ds}^{on}$ at the end. As V_{ds} decreases, V_{gs} remains constant at

$$V_{gs} = V_{th} + \sqrt{\frac{I_o^{on} L}{m \mu_n Z}} \tag{3.8}$$

where I_o^{on} is the maximum I_d. When V_{ds} reaches its on-state value, C_{dg} will be approximately zero. The gate charge flows to C_{gs} and V_{gs} increases again with increasing gate charge.

3.2 Gate-Charge Technique

Prior to irradiation, C_{gs} and C_{dg} relate V_{gs} to the gate charge. Figure 3.4 illustrates the physical arrangement of the capacitors in the MOSFET. Radiation adds interface traps to the Si/SiO_2 interface. The traps add the capacitance C_{it} as shown in Fig. 3.4. C_{it} becomes filled when the traps capture charge carriers from the channel. Placing charge on the gate sweeps the channel Fermi level through the energy range containing the interface trap energy levels. As the Fermi level rises above the trap energy level, the trap will capture an electron.

Figure 3.2 illustrates a gate-charge measurement. Point 'A' labels the first knee point of the gate-charge curve in Fig. 3.2. Before irradiation, Eq. (3.5) describes the region below the knee point of the gate-charge curve. Using Eq. (3.5), V_{gs} at the first knee point is given by

$$V_{knee}C_{gs} = Q_{knee}. \tag{3.9}$$

where V_{knee} and Q_{knee} are the gate-to-source voltage and gate charge at the first knee point respectively. The first knee point represents the point when the channel resistance falls to $R_{ds}^{knee} = \frac{V_{ds}}{I_o^{on}}$. This occurs when the charge-carrier density in the channel inversion layer rises to

$$\frac{L}{R_{ds}^{knee} q \mu_n A} = n \tag{3.10}$$

where n is the charge-carrier density in the channel inversion layer, L is the channel

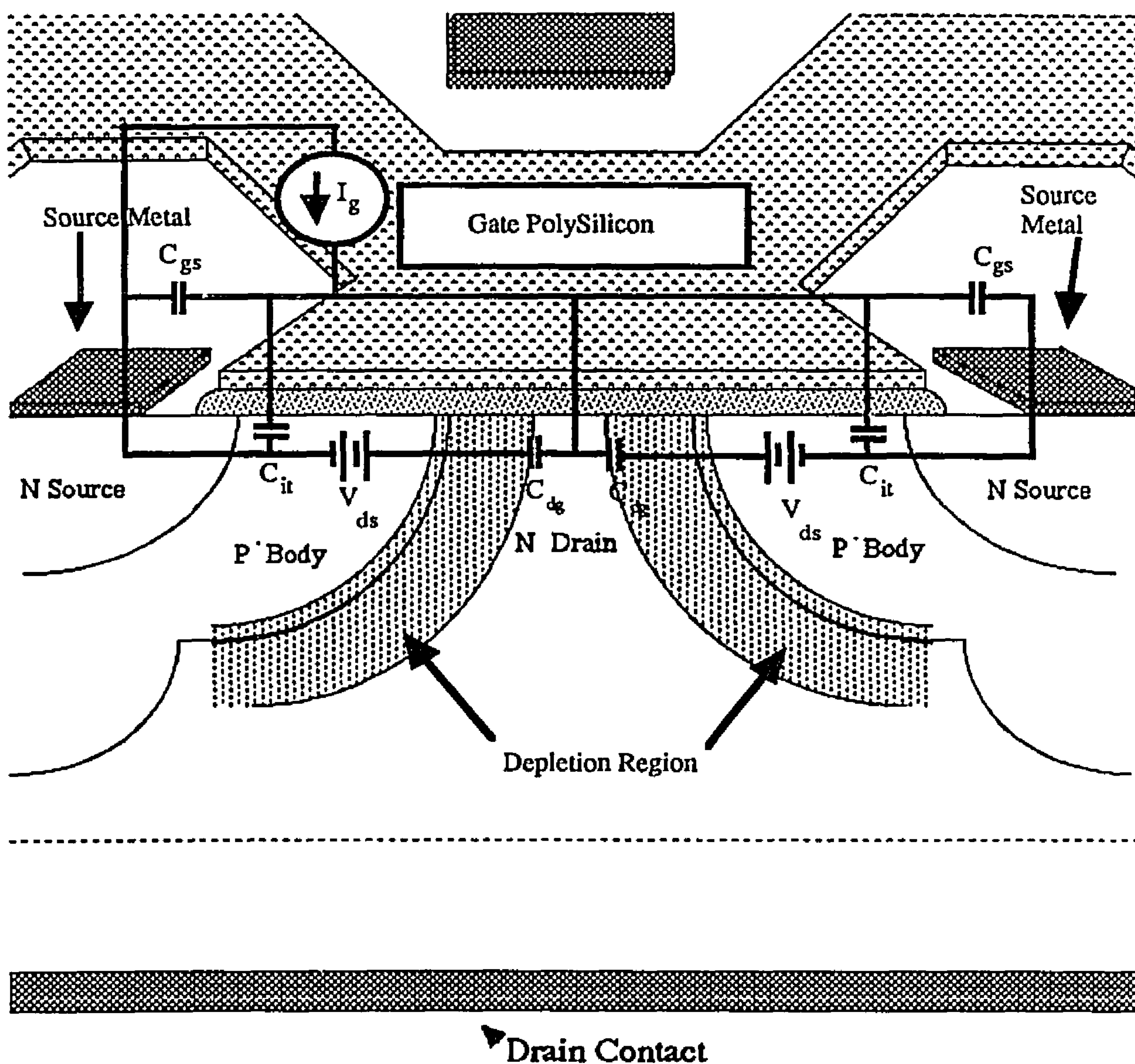

Figure 3.4 - Physical layout of the enhancement-mode n-channel DMOS transistor including the capacitances C_{dg}, C_{gs}, and C_{it}.

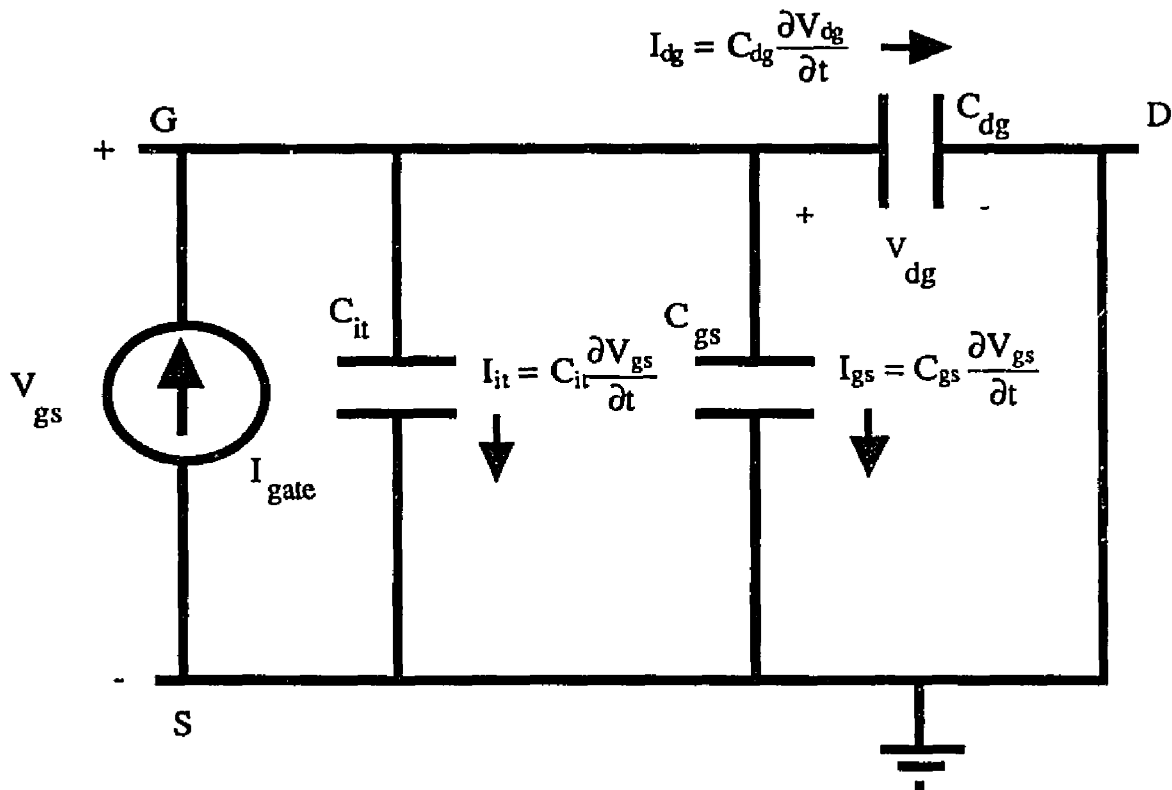

Figure 3.5 - Equivalent circuit for an irradiated MOSFET.

trapped at the interface. Since the trapped charge is not free to move, it can not contribute to the charge density in the channel. Q_{gs} is the charge which contributes to the charge-carrier density in the channel. If Q_{gs} can be found, then by subtracting Q_{gs} from the value of Q'_{knee} as found after irradiation will yield Q_{it}.

Figure 3.6 is an idealized gate-charge curve with interface traps. The regions of constant slope in Fig. 3.6 represent the regions where the capacitance is due to C_{gs}, which is constant. The value of the constant slope is found from the pre-radiation curve. The regions where the slope varies result from the filling of the interface traps, which varies depending on the channel Fermi level. Figure 3.7 illustrates the interface-trap distribution in energy for the device which produced the gate-charge curve in Fig. 3.6. The region around mid-gap in Fig. 3.7 is mostly devoid of interface traps. Due to the fact that the distribution of interface traps is split, the traps will fill in two separate regions of the gate-charge curve. The region labeled 'D' in Fig. 3.6 is where the donor-like traps are filled and the region labeled 'A' in Fig 3.6 is where the acceptor-like traps are filled. The line labeled 'No N_{it}' is fit to the lower part of the curve. The slope here is constant and due to C_{gs}. This line represents what the gate-charge curve would be if there were no interface traps. The line 'P' is fit to the plateau region of the gate-charge curve. The two lines intersect at point '1'. The gate charge at point '1' is the charge on C_{gs} which lowers the channel resistance to R_{ds}^{knee}. The traps add the capacitance C_{it} which must be filled in addition to C_{gs}. At the point labeled '2' both C_{gs} and C_{it} have been filled. The distance from point '1' to point '2' represents the charge which flowed into the interface traps. The total number of acceptor-like traps can be found in Fig. 3.6 by using the line labeled 'Acc Only'. This line is parallel to the line 'No Nit' but it does not include the donor-like traps.

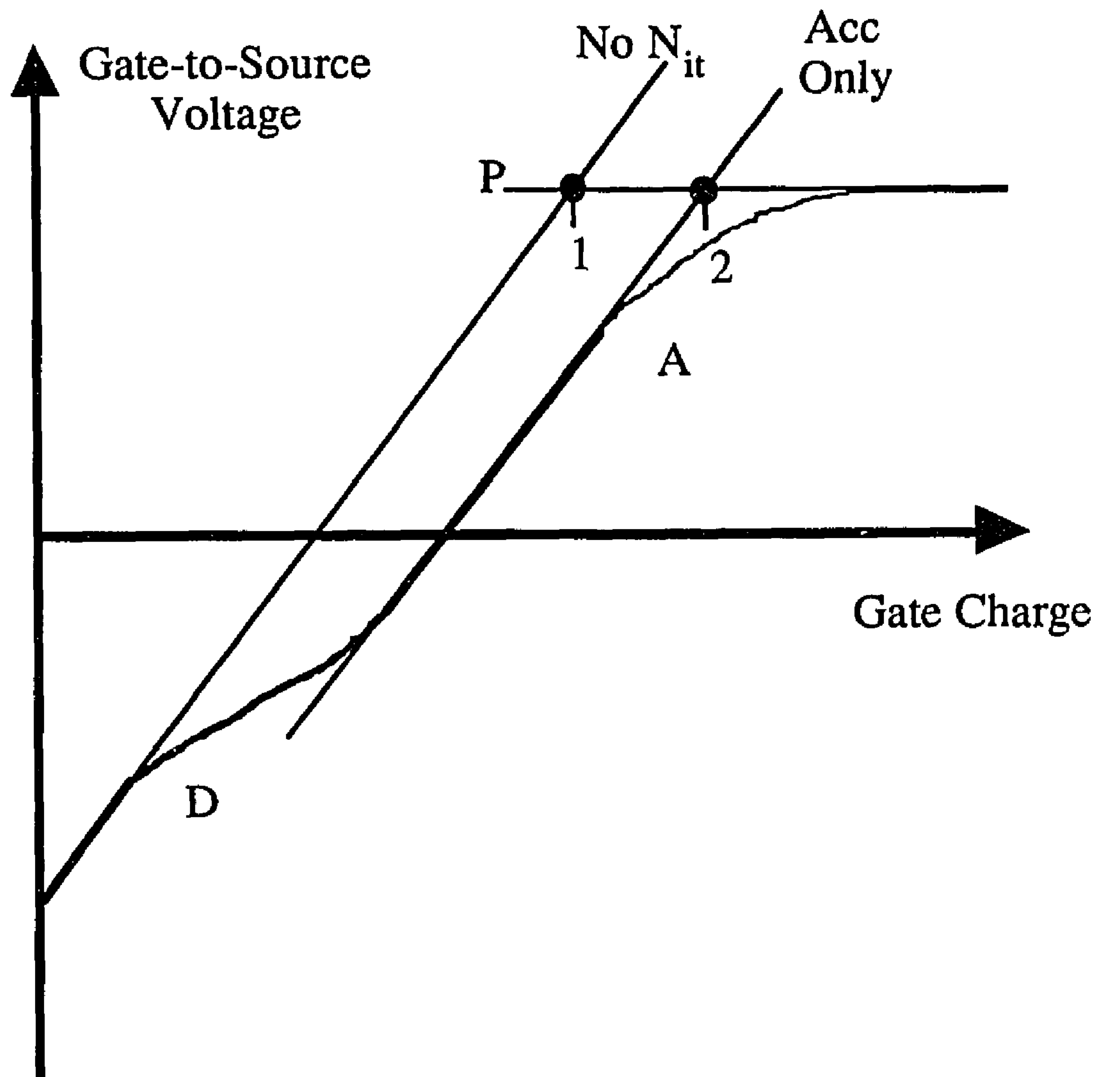

Figure 3.6 - Idealized gate-charge curve illustrating the effects of interface traps.

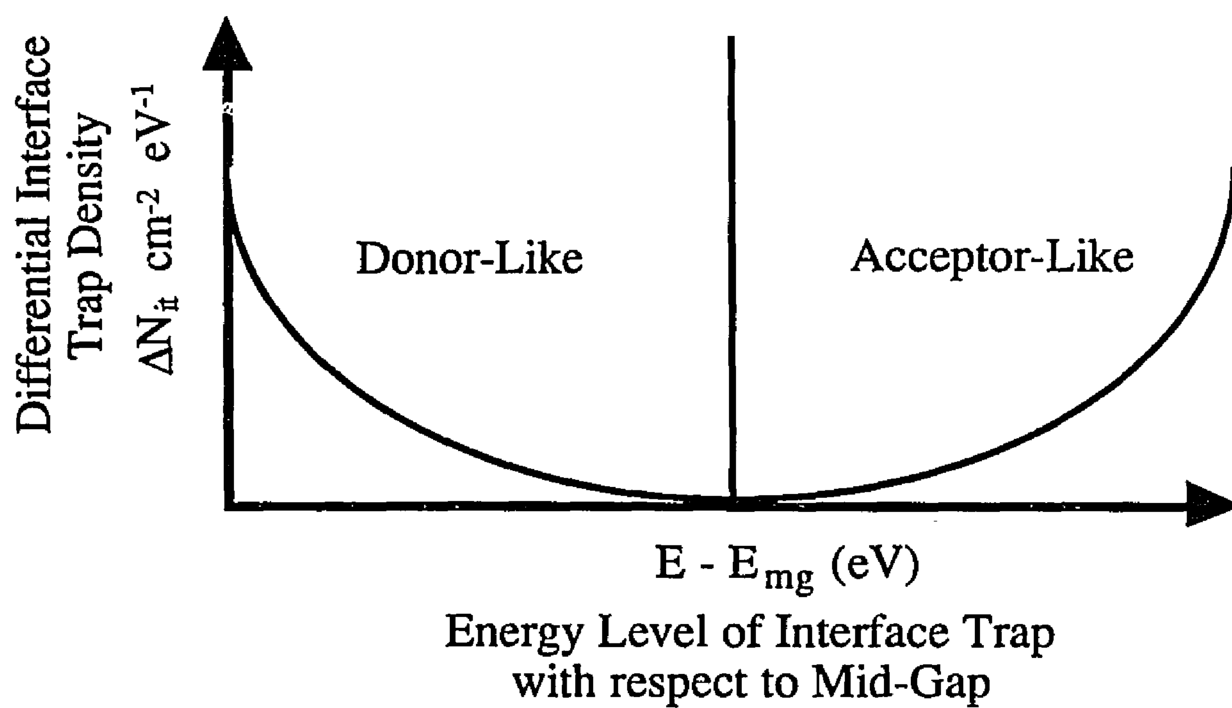

Figure 3.7 - Differential interface trap distribution in energy.

The total charge which flowed into the acceptor-like interface traps is the distance along line 'P' from the line 'Acc Only' to the point '2'. The charge which flowed into the donor-like states is the distance along line 'P' from the line 'No N_{it}' to 'Acc Only'.

Figure 3.8 illustrates a gate-charge curve taken on a DMOS transistor before and after irradiation. The post-radiation curve is shifted so that the first knee points for both curves coincide. In Fig. 3.8, the slope of line 'A' is the same as the slope of the pre radiation curve. Line 'A' represents the slope that the post radiation curve would have if there were no interface traps. The post radiation curve has only one region where the slope varies. This is due to the fact that all of the donor-like traps lie below mid-gap. Mid-gap for this device is ~ -1 V, which places the variation in slope due to the donor-like traps off of the gate-charge plot. Thus, only the filling of the acceptor-like interface traps is shown. The distance along line 'B' from the intersection of 'A' and 'B' to the first knee point is the charge which flowed into the acceptor-like traps.

Figure 3.9 illustrates the gate-charge curve before and after 500 Krad(Si) of radiation. The point V_1 is the V_{gs} corresponding to the plateau region. The shift in the V_1 results from the oxide and interface charge shielding the channel region from the gate. This shift is analogous to the threshold shift seen in MOSFETs. Extra charge must be placed on the gate to offset the charge in the oxide and at the interface. The total number of oxide charges is found by subtracting the shift in the plateau region from the total number of interface traps found previously. This method for finding the number of oxide charges is similar to the method used by the mid-gap technique for finding the number of interface charges.

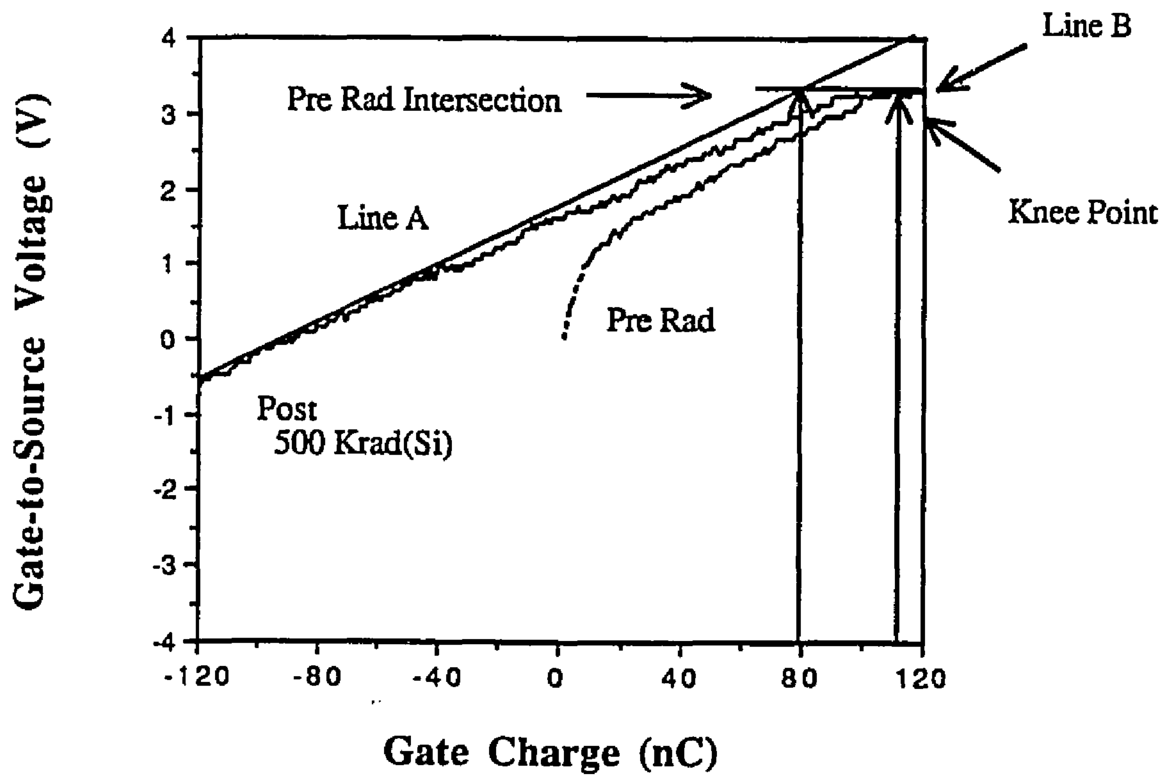

Figure 3.8 - Gate-charge curve taken from an IRH254 DMOS transistor before and after irradiation with the post radiation curve scaled.

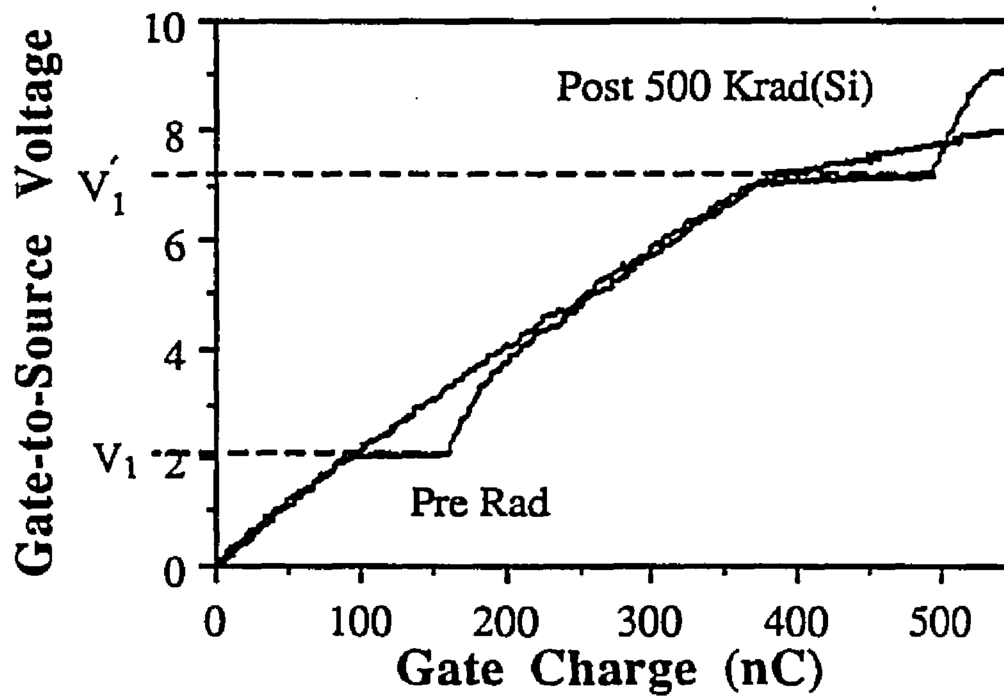

Figure 3.9 - Gate-charge curve taken from an IRH254 DMOS transistor before and after irradiation without the post radiation curve scaled.

The gate-charge curve contains a plateau region where there is no increase in V_{gs} for a corresponding increase in gate charge. This region results from the discharge of the space-charge region associated with the drain-to-body depletion region. Interface traps will lengthen the plateau in a DMOS structure. In a DMOS structure (Fig. 3.4), the gate oxide extends over the drain region. This allows interface traps to be generated at the interface between the gate oxide and the drain region. During a gate-charge measurement, the drain region is held at a positive potential. Since the gate contact is initially grounded, the drain-to-gate voltage (V_{dg}) becomes positive, resulting in an electric field across the oxide which lies over the drain region. The acceptor-like traps which lie in energy below the Fermi level set by V_{dg} are charged negatively. The charged interface traps will act like a capacitor in parallel with C_{dg}. When the space charge region discharges into the channel, the interface traps will become neutral and the extra charge flows into the channel. The increase in the length of the plateau region results from the extra interface charge. The amount of increase reflects the extra charge discharged into the channel region from the interface traps in the oxide above the drain region.

3.3 Gate-Charge Error Due to Large Oxide Charge Build-up

In Chapter Two, the mid-gap technique was shown to have an error of 50% for the interface component of the threshold shift if there was a 5% error in the oxide-charge component when the oxide charge far outnumbered the interface charge (section 2.3). The error is possible since the mid-gap technique first finds the shift due to oxide charge. The oxide charge is much larger, in some devices, than the interface component. If $V_{ot}>>V_{it}$, a 5% error in V_{ot} will result in a much larger error in V_{it}, when using the mid-gap

method. But the gate-charge method first arrives at an answer for V_{it} and then finds V_{ot}. Since (for most commercial devices) $V_{it} \leq V_{ot}$, a 5% error in V_{it} from the gate-charge method will result in at worst a 5% error in V_{ot}. At best, the error in V_{ot} will be much less than 5%.

3.4 Data Extracted by the Gate-Charge Method

Figure 3.10 illustrates the interface charge versus total dose for an irradiated IRH254 transistor found from the gate-charge method. The IRH254 used was the same transistor which was analyzed with the mid-gap method in Chapter Two. In the next chapter, the data in Fig. 3.10 are compared to the data obtained using the mid-gap method.

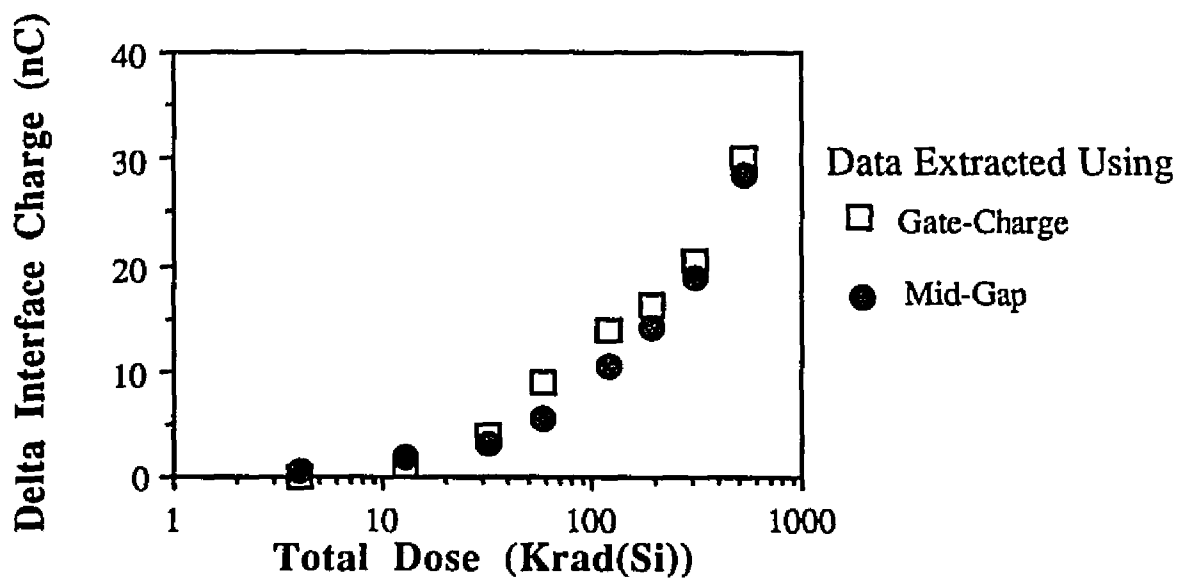

Figure 3.10 - Increase in interface charge found using the gate-charge method versus total dose of radiation from an IRH254 DMOS transistor plotted with the data from the same transistor from Chapter Two.

The gate-charge technique should provide a more accurate method for analyzing the production of ionizing-radiation-induced interface traps and oxide charge when compared to the mid-gap method. The accuracy of the gate-charge method was tested by comparing the interface trap densities obtained from irradiated DMOS structures by the mid-gap method to the densities found by the gate-charge method. The differences found between the two methods were correlated to the errors observed by a computer simulation of the mid-gap method.

CHAPTER IV
COMPARISON BETWEEN MID-GAP AND GATE-CHARGE METHODS

To compare the mid-gap method to the gate-charge method, a radiation experiment was performed on six transistors. The interface charge as found by the mid-gap method was compared to the interface charge as found by gate-charge method. Three IRH254s were irradiated with gamma rays at a dose rate of 200 rad(Si)/min. The total dose on the IRH254s was 550 Krad(Si). Three IRF440s were also irradiated with gamma rays at a dose rate of 200 rad(Si)/min. The total dose on the IRF440s was 35 Krad(Si). The total dose for the IRF440s was held to only 35 Krad(Si) because the devices began operating like a depletion-mode device at this point. In commercial devices such as the IRF440, the oxide trapped charge is much greater in magnitude than the interface charge. The oxide charge (which is positive) shifts the gate-charge curve to the left. If the gate-charge curve is shifted to far to the left, the device will operate as a depletion-mode device and the first inflection point (V_1) will occur at negative gate charge. To reach this area when V_1 is at a negative gate-charge, the gate must be charged negatively prior to performing the gate-charge curve. This can be accomplished, but the experimental setup did not have the capability to bias the devices negatively.

At regular intervals during irradiation, the gate-charge curve, subthreshold curve and above-threshold curve were taken from the irradiated devices. After irradiation, the gate-charge method and mid-gap method were used on the collected data.

4.1 Data from a Typical Transistor

The threshold voltage shift versus total dose for one IRH254 which was irradiated

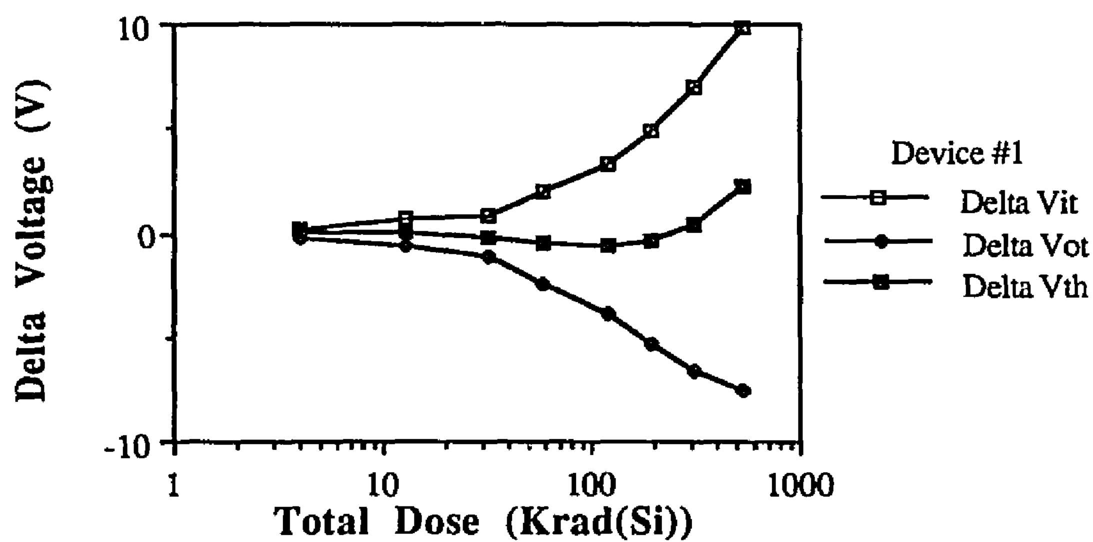

Figure 4.1 - Plot of the threshold voltage shift resolved into the interface and oxide charge components using the mid-gap method versus total dose of radiation for an IRH254 DMOS transistor.

following the procedure in appendix A is shown in Fig 4.1. The data for the remaining five transistors are presented in appendix B. The threshold voltage was resolved into the oxide and interface components by employing the mid-gap method as outlined in appendix A. Figure 4.2 is a plot of the increase in interface charge at threshold versus total dose for the IRH254. The interface charge was found from the interface component of the threshold shift by

$$\Delta Q_{it} = \frac{\Delta V_{it}}{C_{ox}} \tag{4.1}$$

where C_{ox} is the oxide capacitance. The oxide capacitance was found from the data sheets for the IRH254 to be 3400 pF.

Figure 4.3 illustrates the increase in interface charge versus total dose for the IRH254 as found by the gate-charge curve following the outline of Chapter three.

Figure 4.4 compares the amount of interface charge as found from the mid-gap method to the amount of charge found from the gate-charge technique for all of the transistors. If the gate-charge and mid-gap methods produced the same answer for a given total dose, then all of the points in Fig. 4.4 should fall on the 'zero error' line. The best fit of all of the data points is the 'best fit' line. The slope of this line is 0.81. Thus for a given total dose, the mid-gap technique found an amount of interface charge which was 0.81 times the number as found from the gate-charge technique. This difference is explained in the next section as an error from the mid-gap method. A computer simulation of the mid-gap method found that the method underestimates the interface charge by approximately 20%.

4.2 Computer Simulation of Mid-Gap Method

A computer simulation of the mid-gap method was performed as outlined in Chapter

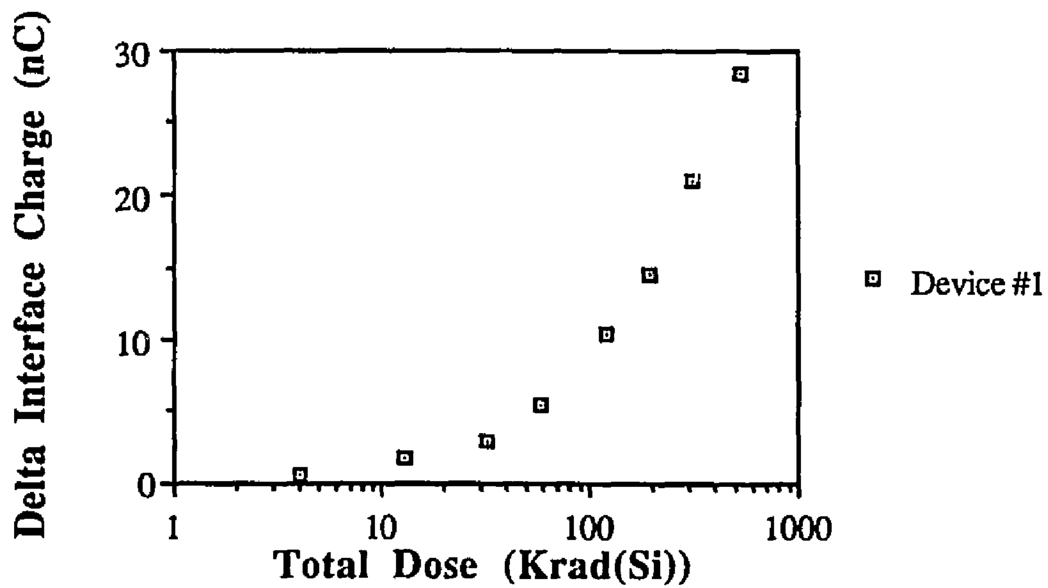

Figure 4.2 - Increase in interface charge found using the mid-gap method versus total dose of radiation from an IRH254 DMOS transistor.

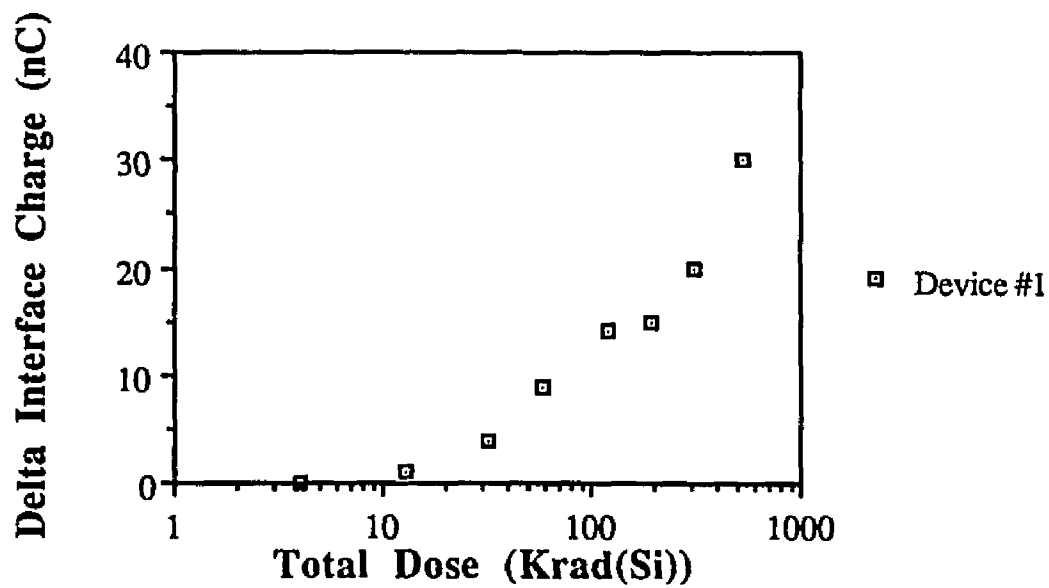

Figure 4.3 - Increase in interface charge found using the gate-charge method versus total dose of radiation from an IRH254 DMOS transistor.

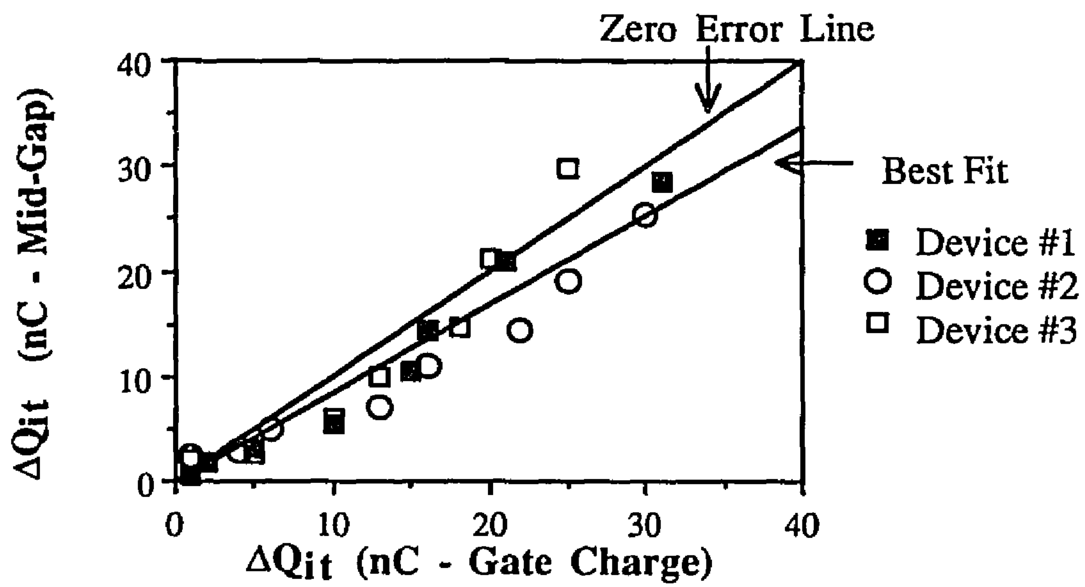

Figure 4.4 - Comparison of interface charge found using the mid-gap method to the interface charge found using the mid-gap method.

Two. Subthreshold I-V characteristics of MOSFETs with and without interface traps were produced from the analytic equations given in Chapter Two. The mid-gap method was then used on these simulated characteristics to extract the oxide and interface charge densities. The ratio of the known interface-charge density divided by the interface-charge density found by the mid-gap method is plotted versus increasing interface-charge density in Fig. 4.5. This figure was generated by employing the mid-gap method on simulated subthreshold curves which were produced with increasing interface-charge density. The ratio rises to an approximately constant 1.23 (or 19%) for most interface charge densities. The error bars on Fig. 4.5 represent a ±5% error which is approximately the resolution limit of the 4145b parametric analyzer.

Assuming that the gate-charge technique is a valid technique which accurately measures ΔQ_{it}, then the slope of the line indicates the error associated with the mid-gap technique. The slope of the best line-fit to all of the data points is 0.81 which corresponds to an error of 19%. This is in approximate agreement with the 19% error predicted by the computer simulation.

4.3 Summary

The mid-gap method and gate-charge method were seen to yield interface trap densities which differed by a factor of 0.81 after irradiation. The computer simulation of the mid-gap method indicated that the mid-gap method underestimates the interface trap density by a factor of approximately 0.80.

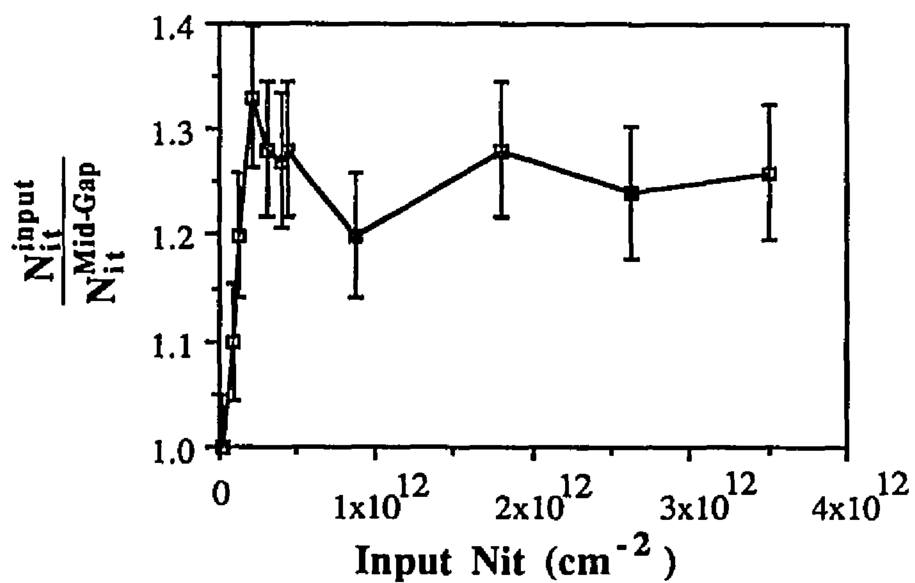

Figure 4.5 - Plot of the ratio of the known interface-charge density divided by the interface-charge density found by the mid-gap method versus interface charge used in the simulation of the subthreshold region.

CHAPTER V
SUMMARY AND CONCLUSIONS

5.1 Summary of Thesis

When electronic circuits containing MOS technologies are placed in space environments, MOSFETs are subjected to ionizing radiation. The ionizing radiation produces EHPs in the gate oxide of the MOSFETs. The holes recombine at recombination centers and liberate H^+ ions. The H^+ ions travel to the Si/SiO_2 interface and produce interface traps. The holes which do not recombine find trapping sites in the oxide. The oxide and interface charge produce alterations in the transfer characteristics of the MOSFET. Experimental techniques have been proposed to extract the number of ionizing-radiation-induced interface and oxide charges from the transfer characteristics of the MOSFET. The mid-gap technique is today the most widely used method for extraction. The mid-gap method correlates the above-threshold voltage shift after irradiation to the number of oxide and interface charges. The subthreshold I-V relationship is used to find the shift in the mid-gap voltage after irradiation. The shift in V_{mg} is correlated to the number of oxide charges. The successful implementation of the mid-gap technique relies on the linear nature of the subthreshold transfer characteristic which is used to extrapolate the curve to mid-gap. The subthreshold transfer characteristic does not remain linear after irradiation due to the dependence of the charged interface trap and the channel mobility on the gate voltage. A computer simulation of the subthreshold transfer characteristic illustrated an error of approximately 20% in the mid-gap method resulting from the introduction of interface traps in the model for a MOSFET. If the magnitude of V_{ot} rises significantly above the magnitude of V_{it}, the mid-gap method suffers from the effect of the oxide-charge component swamping out the interface-charge component.

The gate-charge technique uses the dependency of the charged interface traps on the gate voltage to find the total number of charges which will flow into ionizing-radiation-induced interface traps. The interface traps add a capacitance to the gate capacitance. The interface capacitance alters the slope of the gate-charge curve. The extra charge which flows into the interface capacitance is found by matching the slope of the pre-radiation gate-charge curve to the post-radiation curve. The distance between the post-radiation curve and the slope of the pre-radiation curve is the charge which entered the interface traps. The first knee point of the gate-charge curve shifts after irradiation. The shift in V_{gs} for the first knee point is used to find the sum of the oxide and interface charge. By subtracting the interface charge from the shift in the first knee point, the number of oxide charges is found. Since the gate-charge method first arrives at a result for the interface charge, the gate-charge method does not suffer from the effect of the oxide charge swamping out the interface charge. The mid-gap method must extrapolate the subthreshold curve back to the mid-gap voltage. The gate-charge method does not required the extrapolation of a curve into an experimentally unmeasurable area.

The length of the plateau region in the gate-charge curve represents the charge stored on C_{dg}. After irradiation, interface traps are generated in the oxide which extends over the drain region in the DMOS transistor. These interface traps add a capacitance in parallel with C_{dg}. This capacitance increase C_{dg} which leads to an increase in the length of the plateau region. While this effect does not yield important information for those interested in charge separation, this information is useful for circuit designers who use C_{dg} as a design parameter.

5.2 Conclusions

The mid-gap method has been used to separate the effects of ionizing-radiation-induced

interface and oxide charge effects from the I-V characteristics of the MOSFET. The interface charge alters the linear nature of the subthreshold log(I)-V characteristic. A non-linear nature of the subthreshold log(I)-V curve invalidates one of the procedures of the mid-gap method. The gate-charge technique does not require extrapolations. Since the gate-charge curve first finds V_{it}, the gate-charge curve does not suffer from the oxide charge effect swamping out interface charge effects. The gate-charge curve produces useful information about the interface charge production in the oxide over the drain region in the DMOS transistor. Since the gate-charge method uses the value for C_{gs} found from the pre-radiation curve, if the pre-radiation curve is not linear before the first knee point, a value for C_{gs} can not be obtained. Without a value for C_{gs} the post radiation curve can not be used to find C_{it}. If the pre radiation curve is taken from a device with a large interface trap component, then the slope of the curve below the knee point will be as non-linear as the post radiation curve. C_{gs} will also be non-linear if the overlap area between the source metal and gate polysilicon is small. If the overlap capacitance is small, then the depletion layer capacitance will dominate. The depletion layer capacitance is non-linear. Without a linear C_{gs}, the gate-charge method can not be used. When C_{gs} is non-linear, the mid-gap method is more useful.

APPENDIX A
EXPERIMENTAL SETUP

A radiation experiment was performed on six DMOS transistors to compare the reliability of the mid-gap and gate-charge techniques. The DMOS structures were irradiated with gamma rays and then the mid-gap charge-extraction technique was compared to the gate-charge-extraction method. The differences found between the two methods were explained as the result of the error in the mid-gap technique.

A.1 Device Types and Bias Conditions

Three IRF440s and three IRH254s were used in the radiation experiment. The IRF440s are DMOS n-channel structures which were designed for commercial use. The IRH254s are DMOS n-channel structures which were designed to be used in a radiation environment. The gate oxides of the IRF440s and IRH254s respond differently to ionizing-radiation. The IRF440s produce a smaller amount of interface traps compared to the IRH254s for a given dose of radiation. The devices were chosen for their range of responses to radiation. A good extraction technique must be able to extract information out of both device types without a large error.

All of the devices were biased positively during irradiation. The positive bias enhances the interface trap production.

All of the devices were irradiated with gamma rays from a Cobalt-60 source at a dose rate of 200 rad(Si)/Min.

A.2 Experimental Equipment for Mid-Gap Technique

A Hewlett-Packard 4145b Semiconductor Parameter Analyzer was used to take all of the I-V measurements for the mid-gap technique. The 4145b is a computer integrated system with four source and measurement units (SMUs). Each SMU can either output a current and read the voltage drop across the output or output a voltage and read the current which is leaving the output. The computer control of the 4145b allows the user to choose two SMUs which are swept through a range of either voltage or currents. The other two SMUs which were not chosen to be swept can have either a constant voltage or a constant current output selected. The machine will then display an X-Y plot of the measured voltage or currents corresponding to any SMU versus any other SMU. The X-Y plot can be displayed in normal, semilog, or log format. After generating the X-Y plot, the data can be stored, manipulated, or curve fitted by the computer.

Figure A.1 illustrates a plot of the drain current versus gate-to-source voltage for an IRF440 in saturation taken prior to radiation. The threshold voltage of the device is found by extrapolating the $\sqrt{I_d}$ versus V_{gs} curve back to the intersection with the V_{gs} axis. The 4145b allows the user to program operations of mathematical functions (such as the square root) on the measured data returned from an SMU. Figure A.2 presents the data in Fig. A.1 after taking the square root of the drain current. Now the curve is linear. The 4145 allows the user to select two points on the X-Y plot which will be fitted to a line. This is done in Fig. A.2. For consistency, the points chosen for all of the curve fits before and after irradiation should correspond to when the channel is operating under the same conditions. The points chosen were when the square root of the drain current equals 100 $mA^{1/2}$ and 200 $mA^{1/2}$. The surface potential in the channel will be approximately the same by choosing the same drain current. The 4145b then fits a line to these points and then calculates the slope, x-axis intercept, and y-axis intercept of the line.

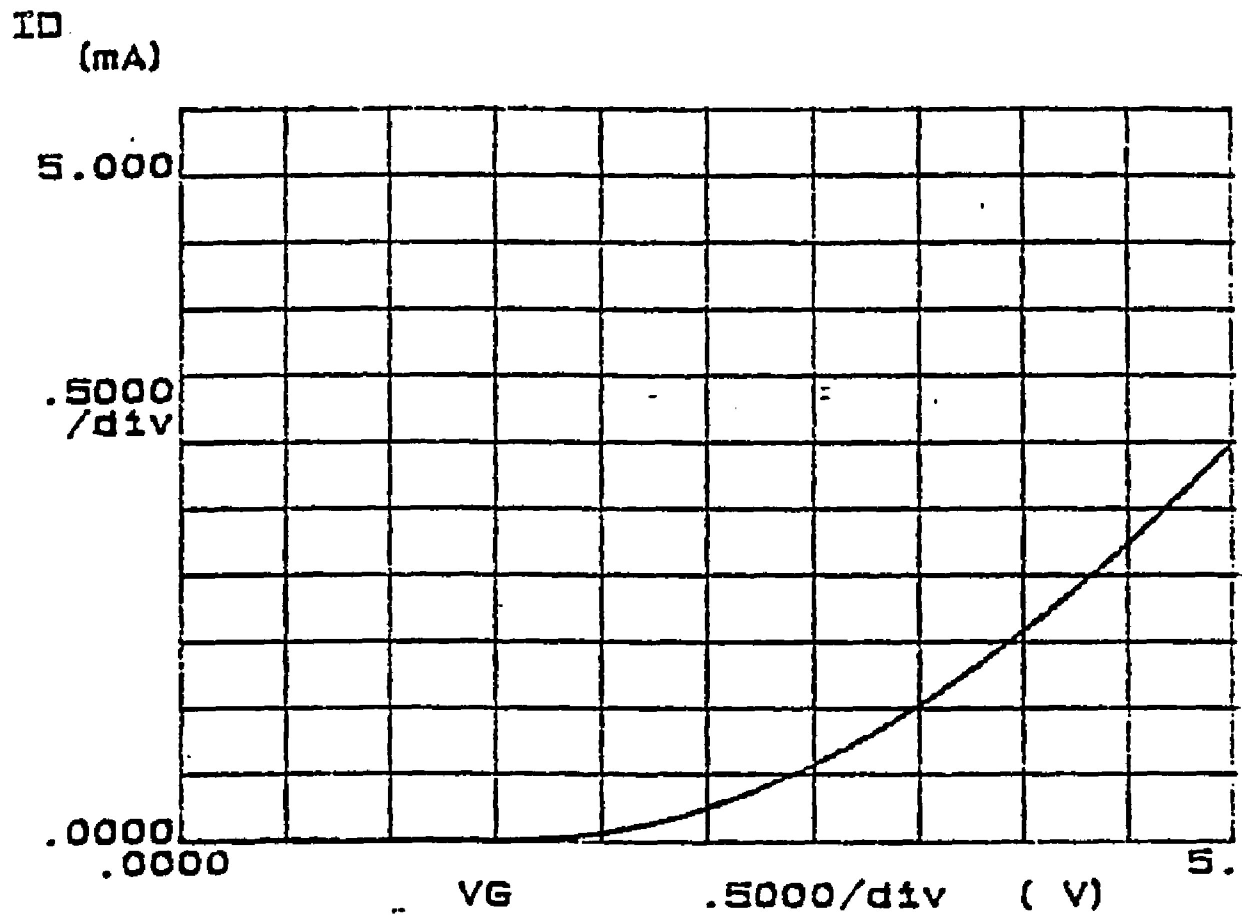

Figure A.1 - Typical above-threshold I-V relationship taken from a transistor using an HP4145b parameter analyzer.

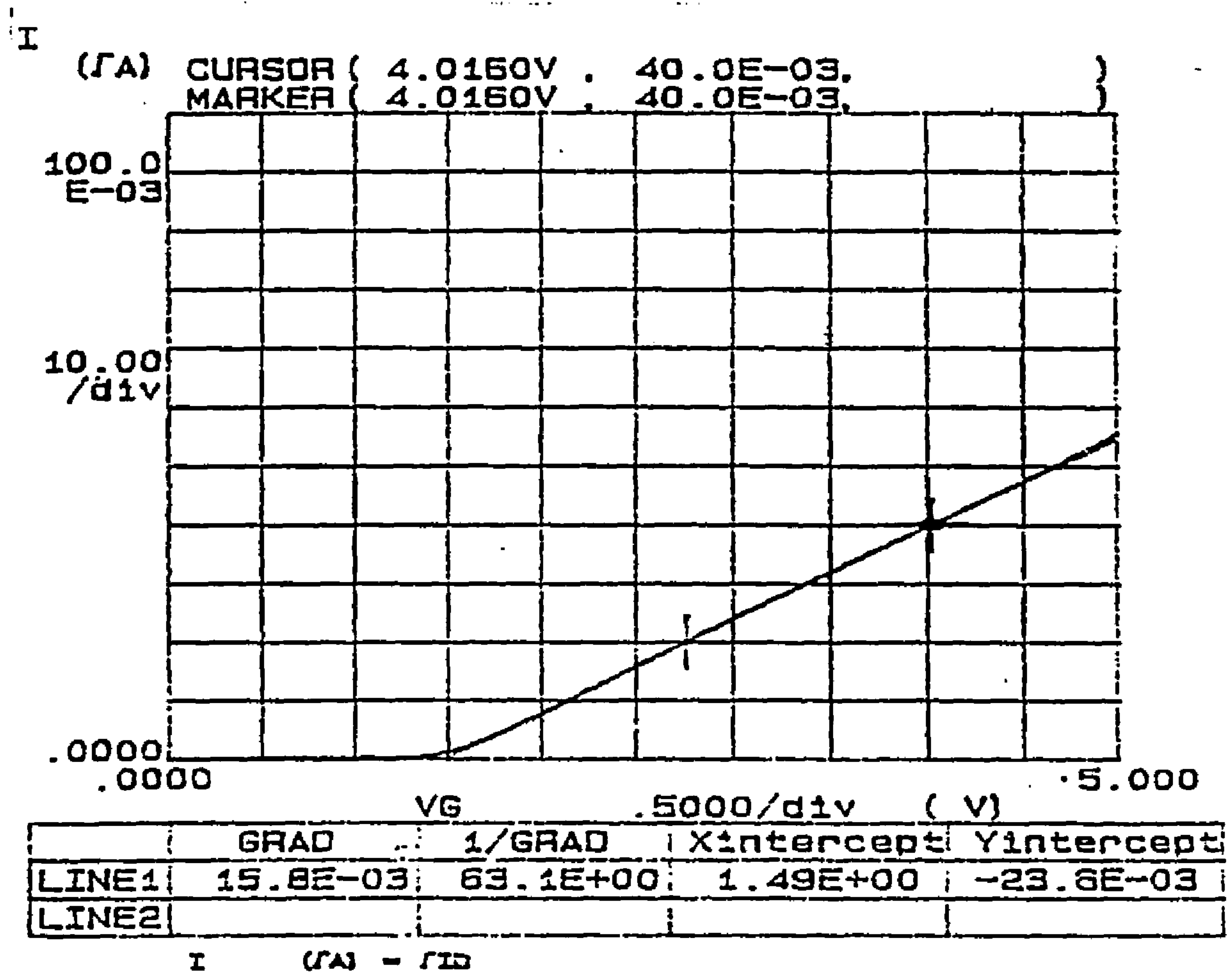

Figure A.2 - Figure A.1 plotted as the square-root of the drain current versus gate voltage.

The 4145b then displays the results on the plot.

Figure A.3 illustrates the subthreshold $\log(I_d)$ versus V_{gs} curve. The mid-gap method uses the linear nature of the $\log(I_d)$ versus V_{gs} curve to extrapolate the curve back to the current which flows when the Fermi level is in the middle of the band-gap. The current which flows at that point can be determined theoretically. A line is fit to the subthreshold curve in Fig. A.3. The points chosen for the curve fit were 1 μA and 100 nA. The 4145b calculates the slope of the curve fit. The units of the slope are in decades of current per volt. The slope relates the incremental gate voltage needed to change the drain current by one decade. The 4145b will display on the plot the V_{gs} corresponding to a drain current of 1 μA. The number of decades between the current which flows at mid-gap and 1 μA is found by

$$\text{Number of Decades} = \log\left(I_{mg}\right) - \log\left(10^{-6}\right) \tag{A.1}$$

where I_{mg} is the drain current at mid-gap. If the V_{gs} corresponding to 1 μA is known and the $\log(I_d)$ versus V_{gs} relationship is linear, then the V_{gs} corresponding to mid-gap can be found by

$$V_{mg} = \frac{\text{Number of Decades}}{\text{Slope of Curve Fit}} + V_{gs}(1\ \mu A) \tag{A.2}$$

where V_{mg} is the V_{gs} at mid-gap.

Assuming that the interface traps are neutral at mid-gap, the shift in the mid-gap V_{gs} after irradiation is ascribed to the build-up of oxide charge,

$$\Delta V_{ot} = V_{mg}' - V_{mg} \tag{A.3}$$

where ΔV_{ot} is the voltage shift due to oxide trapped charge, V_{mg}' is the post radiation mid-gap voltage and V_{mg} is the pre radiation mid-gap voltage. The shift due to interface traps which are charged at threshold is found by

$$\Delta V_{it} = V_{th}' - V_{th} - \Delta V_{ot} \tag{A.4}$$

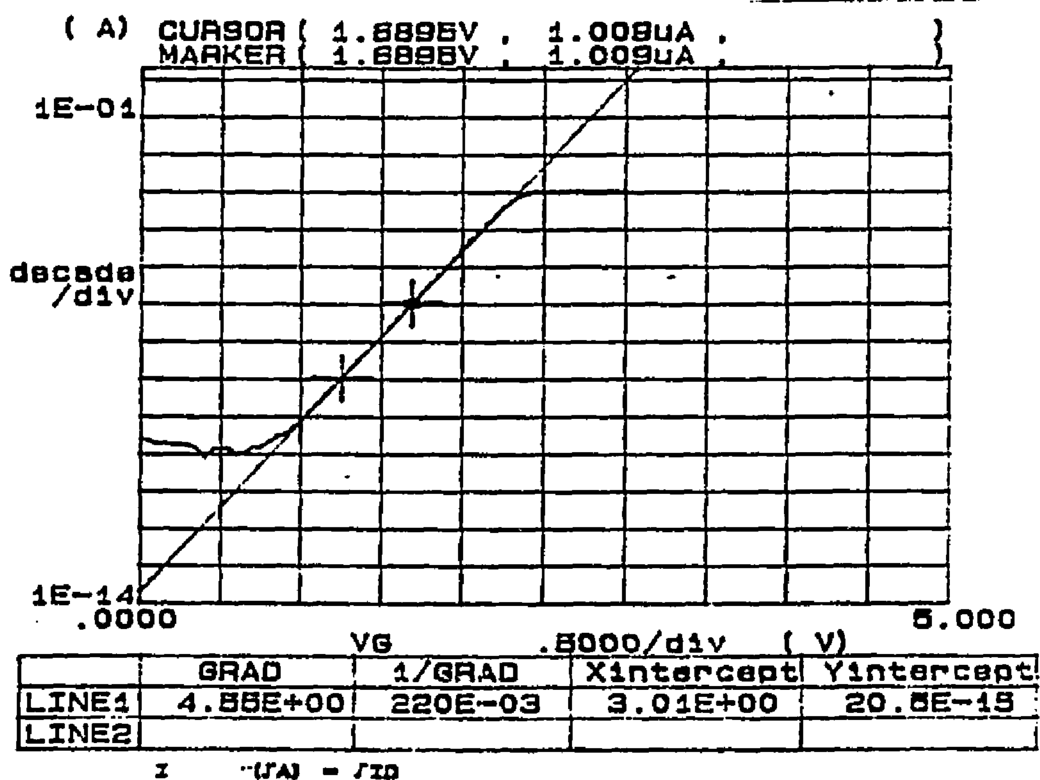

	GRAD	1/GRAD	Xintercept	Yintercept
LINE1	4.55E+00	220E-03	3.01E+00	20.5E-15
LINE2				

Figure A.3 - Typical subthreshold I-V relationship taken from a transistor using an HP4145b parameter analyzer.

where ΔV_{it} is the voltage shift due to interface charge, V'_{th} is the post radiation threshold voltage, and V_{th} is the pre radiation threshold voltage[5].

A.3 Gate-Charge Measurement

A gate-charge measurement requires the ability to measure the gate-to-source voltage with the drain held at a non-zero potential while the gate is charged at a constant rate[14]. Figure A.4 illustrates the experimental equipment used in this experiment. The oscilloscope records the V_{gs} waveform as the gate is charged at a constant rate. Figure A.5 illustrates the circuitry used to switch the current source. Q1 is used as a resistance while Q2 switches the base of Q1. When Q1 is cut off, the current flows into the gate. When Q1 is on, the current from the current source and the gate of the MOSFET is sent to ground.

The drain current of the device under test (DUT) must be regulated. Q3 in Fig. A.3 is a MOSFET used to regulate the current of the DUT. The gate voltage of Q3 sets the maximum current through the DUT, while the variable resistor R1 sets the gate voltage. The capacitor C2 acts to store energy, which lessens the effects of any inductance in the V_{DD} leads.

The DUT is placed in the setup illustrated in Fig. A.4. V_{DD} is set to 60 Volts, the current is regulated to 3.3 Amps, and the current source is set at 10 mA. A signal generator switches the input of Q2 at a frequency of 7 KHz. The oscilloscope records the gate-to-source voltage as a function of time. Multiplying the time base of the oscilloscope by the gate current changes the time base of the oscilloscope to gate charge.

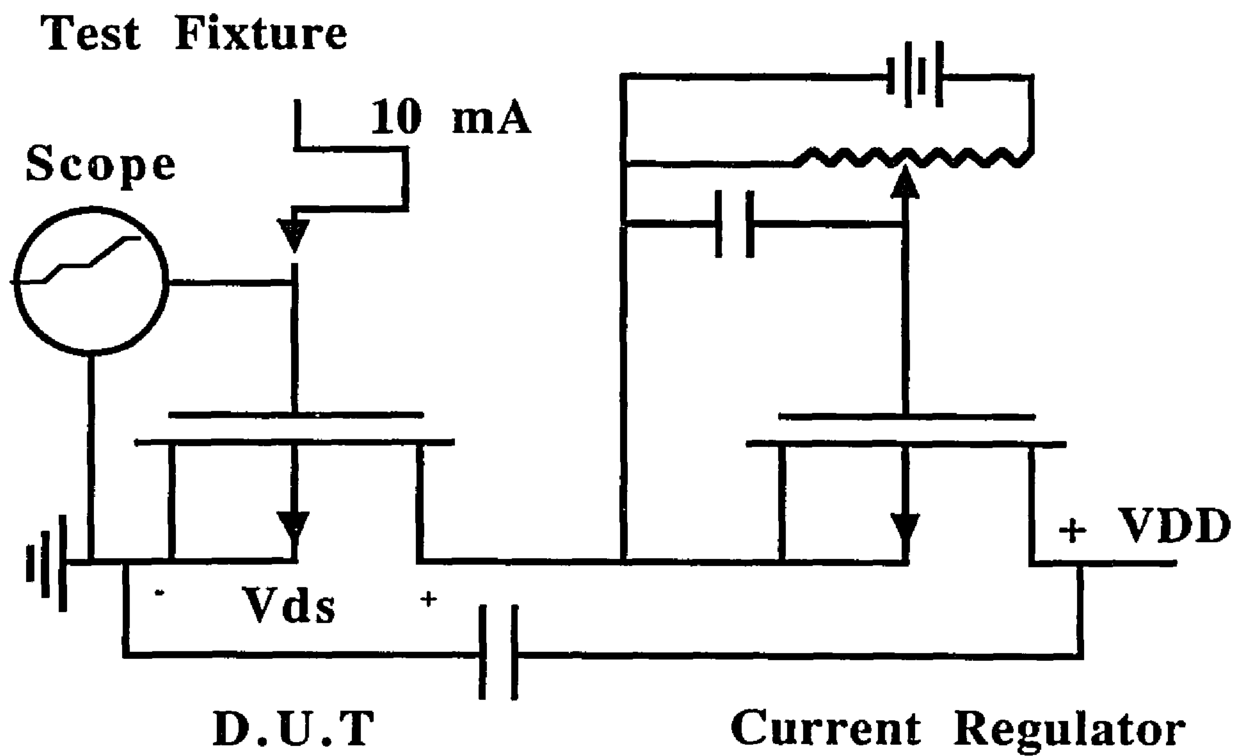

Figure A.4 - Diagram of the experimental setup used to take the gate-charge curve.

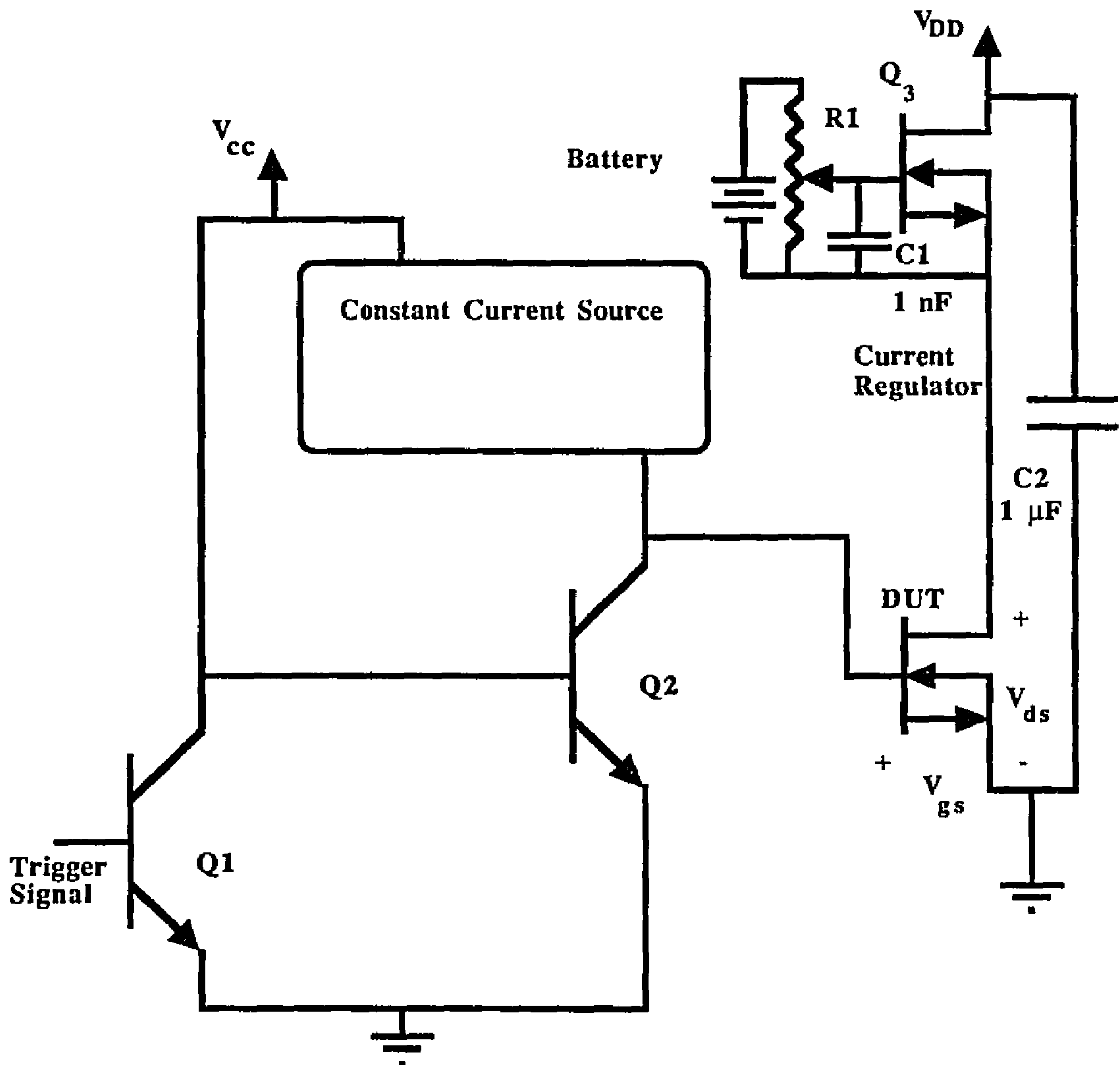

Figure A.5 - Diagram of the circuitry used to charge the gate of the DUT while regulating the drain current.

The time base of the oscilloscope was much larger than the rise time of Q2 so that the oscilloscope would not record any turn-on transients. The constant gate-current source was voltage limited to 11 volts.

A.4 Gate-Charge Technique

Figure A.6 is a gate-charge measurement taken on an IRH254 before irradiation. The first knee point represents the point where the conductivity of the channel is at V_{ds}/I_o where I_o is the regulated current of the regulator. The second knee point represents the point when the drain-to-body depletion capacitance is totally discharged. The jump in the curve after this second knee point results from the effect of inductance in the V_{DD} power supply.

Figure A.7 is a gate-charge measurement taken on the same IRH254 after irradiation. The gate-charge curves were scaled so that the first knee point for the pre and post radiation curves coincided. The production of oxide charge and interface traps causes changes in the gate-charge curve. The interface traps have added a capacitance to the gate of the device. As the V_{gs} is raised on the device, the interface traps will accept electrons. When this happens, the capacitance of the gate is altered. The change in capacitance will change the slope of the gate-charge curve. In Fig. A.7, line 'A' has the same slope as the pre radiation curve and it represents what the slope of the post radiation curve should be if there were no interface traps. Line 'B' is fit to the plateau region. Line 'A' intersects line 'B' at the point where the post radiation curve should intersect the plateau region if there were no interface traps. The distance between the two intersection points is the total charge which flowed into the interface traps.

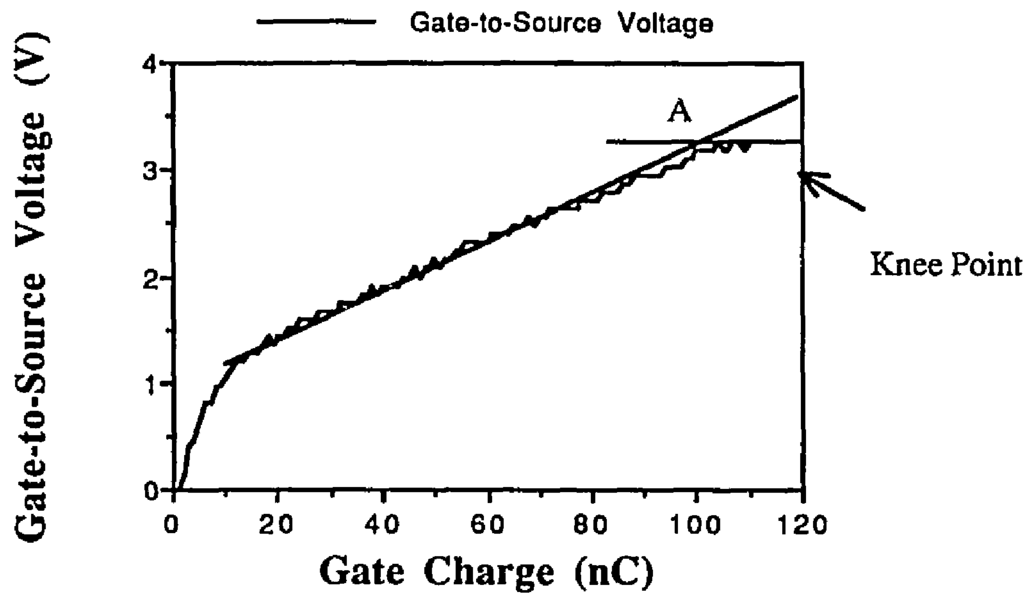

Figure A.6 - Gate-charge measurement taken on an IRH254 before irradiation.

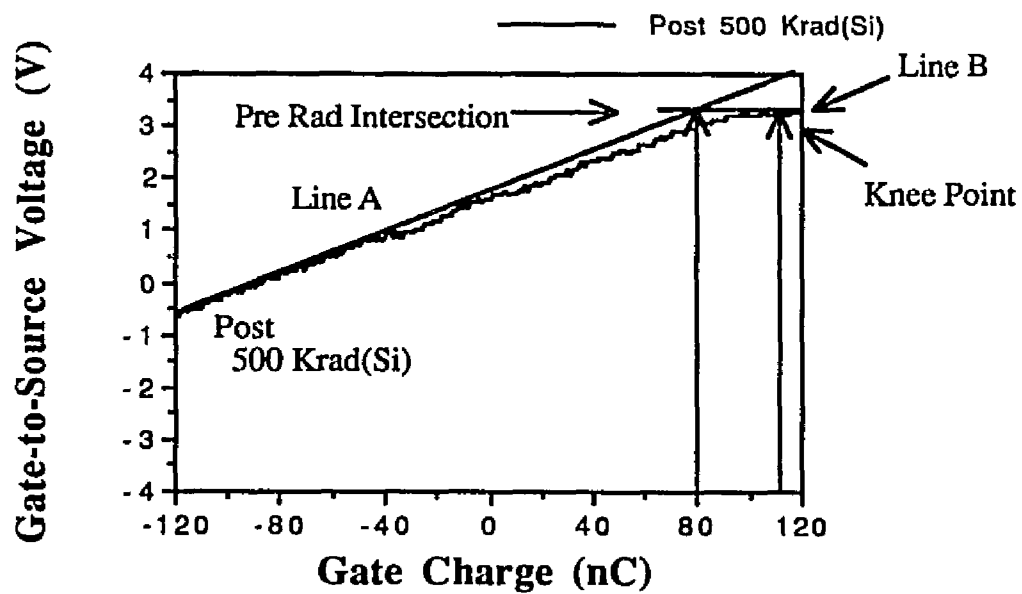

Figure A.7 - Gate-charge measurement taken on an IRH254 after irradiation.

The first knee point represents the point where the channel is strongly conducting. The knee point for the post radiation curve has shifted toward higher gate charge and higher gate-to-source voltage. The shift in the knee point is the result of interface and oxide charge build-up. The number of oxide trapped charges is found by subtracting the total charge which flowed into the interface traps from the shift in gate charge for the knee point.

A.5 The Radiation Experiment

Three devices at a time were irradiated. The devices were placed in a fixture which placed a positive potential on the gate and grounded the source and drain. The fixture was lowered into a lead-shielded chamber which, when closed, was exposed to a Cobalt-60 source which has a dose rate of 280 Rad(Si)/Min at the surface of the source. The devices were set back from the source so that the dose rate received by the fixture was 200 Rad(Si)/Min. After an interval of time, the devices were removed from the source chamber and their above-threshold I-V, subthreshold I-V, and gate-charge curves were taken. Upon the successful completion of the characterization, the devices were subjected to another dose of radiation. Due to the length of time required for the gate-charge measurement (around 6 minutes for three devices) and the desire to minimize the annealing of the devices, only three devices can be irradiated at one time if the characterization is done manually.

A.5.1 Radiation Source

All experiments were done with a Cobalt-60 gamma radiation source in the Nuclear and Energy Engineering Department at the University of Arizona. The source was recently calibrated by the National Bureau of Standards (NBS) to have a dose rate of 280 Rad(Si)/Min at the surface of the source. The calibration was done with a Thermo

Luminescent material which was placed at various positions in the source pit and then exposed to radiation. The TL material was analyzed at to find the dose rate as a function of position in the pit. The dose received by the test fixture can be changed by varying the distance between the fixture and the source. The dose-rate versus distance from the source is described empirically by

$$D = D_{cal}\frac{(7.28\ \text{cm})^2}{(X + 13.03\ \text{cm})^2} \qquad (4.5)$$

where D is the dose rate at a distance X from the source (measured in cm) and D_{cal} is the dose rate found from the NBS calibration.

When the experiment was placed at the appropriate distance from the source, the chamber was sealed by a lead cover. The source is disconnected from the chamber by a lead cover, which is removed when the chamber is sealed to expose the test fixture to radiation.

A.5.2 Test Fixture

Figure A.8 illustrates the test fixture used for the irradiations. The fixture was used to hold physically the devices in place while applying biases to the appropriate terminals. The devices were placed in a circular fashion so that each device would receive the same dose. This assumes that the radiation source had no unusual angular dependence in its output.

A.6 Summary

A radiation experiment was performed on three IRH254s and three IRF440s. The interface and oxide trapped charges were separated using the gate-charge and mid-gap extraction techniques.

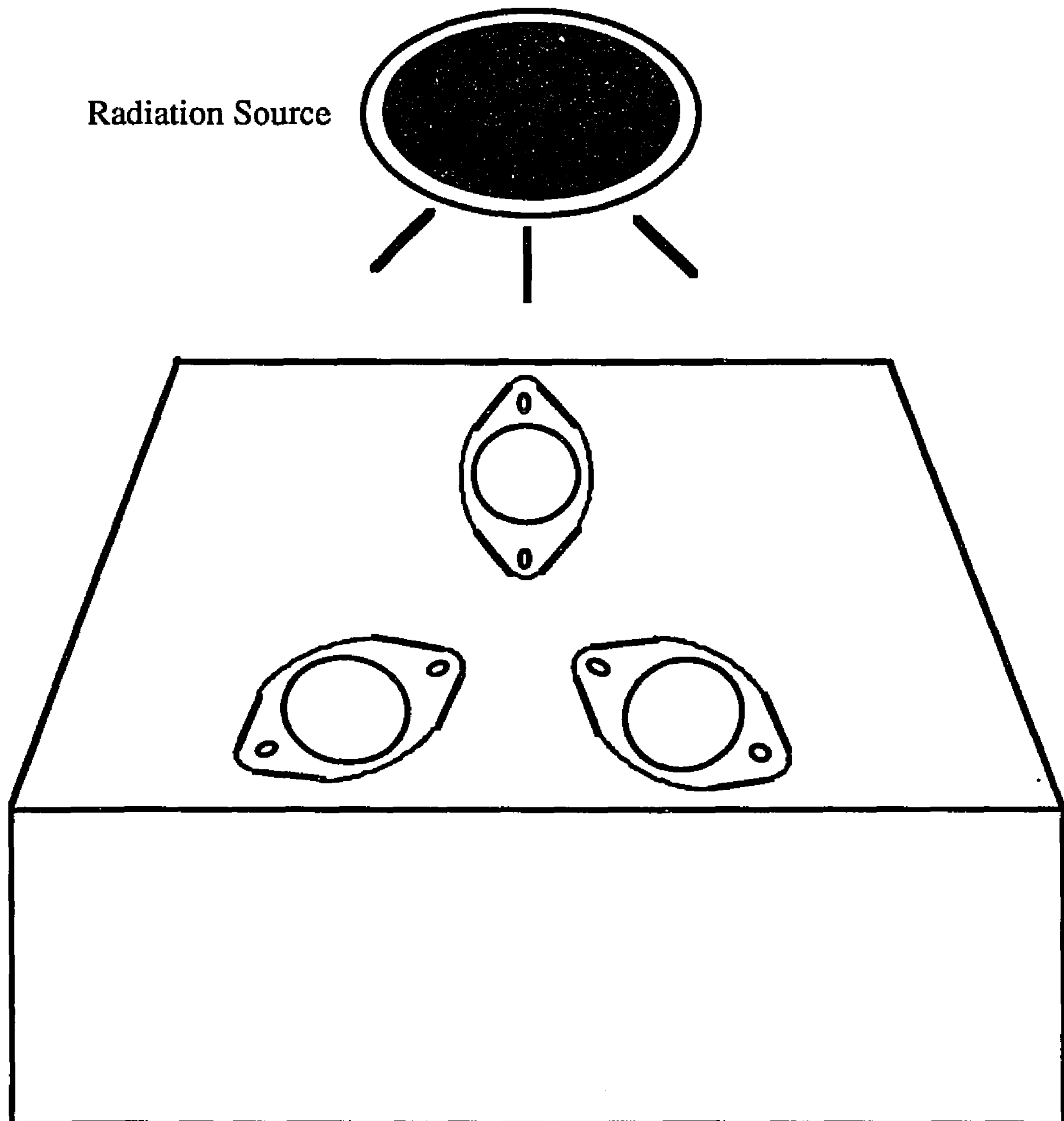

Figure A.8 - Diagram of the radiation test figure.

APPENDIX B
LISTING OF DATA FROM ALL IRRADIATED TRANSISTORS

Data from three IRF440 - Charge separated by mid-gap method 97

Data from three IRH254 - Charge separated by mid-gap method 100

Data from three IRF440 - Charge separated by gate-charge method 103

Data from three IRH254 - Charge separated by gate-charge method 106

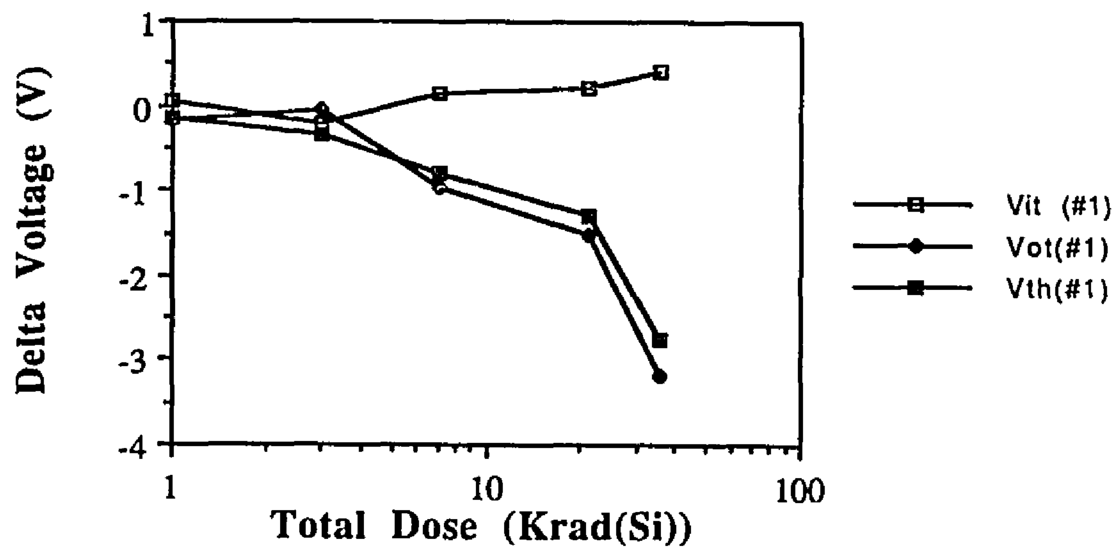

IRF440 Device #1 - Mid-Gap

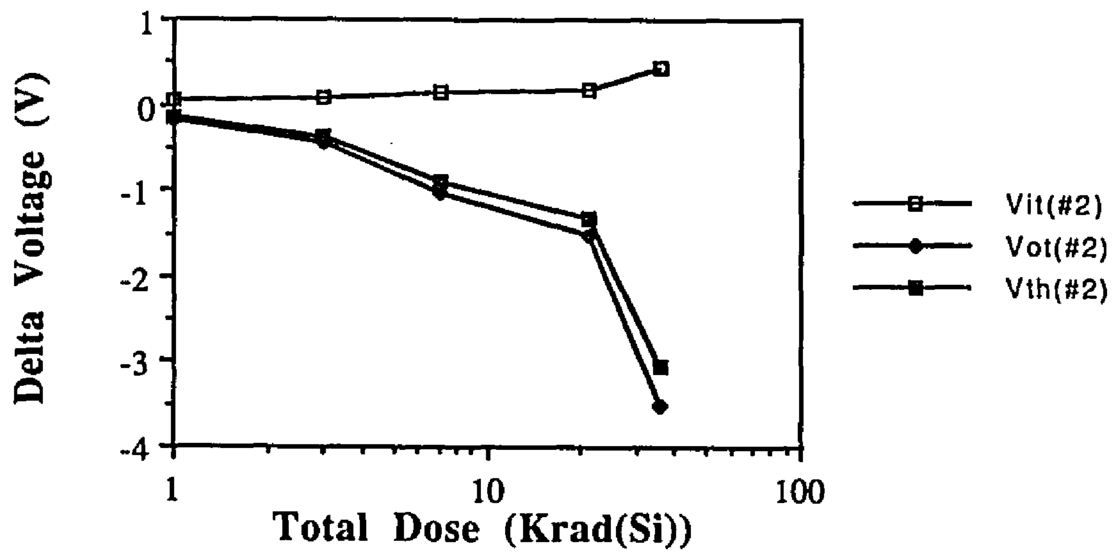

IRF440 Device #2 - Mid-Gap

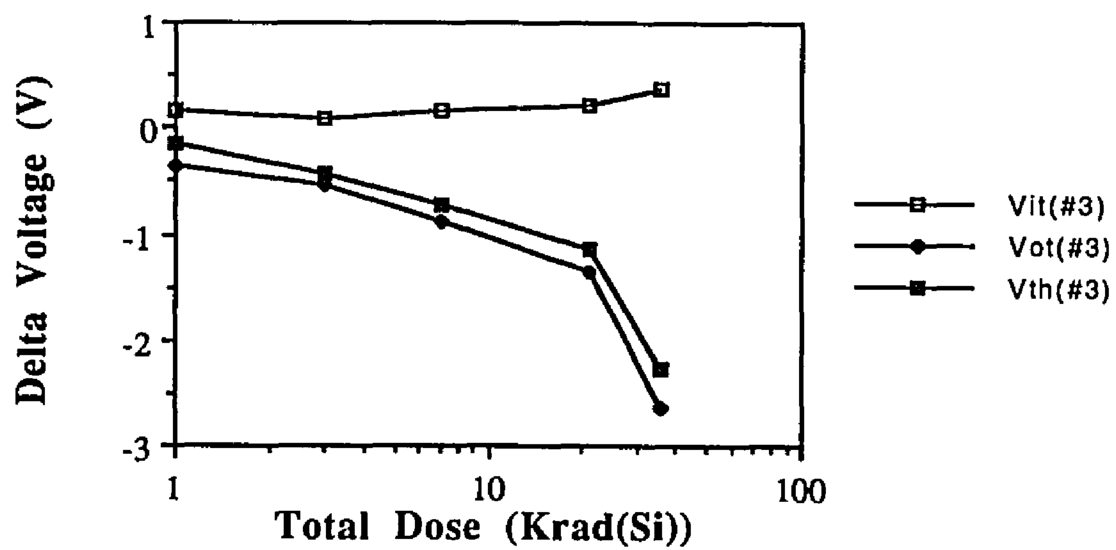

IRF440 Device #3 - Mid-Gap

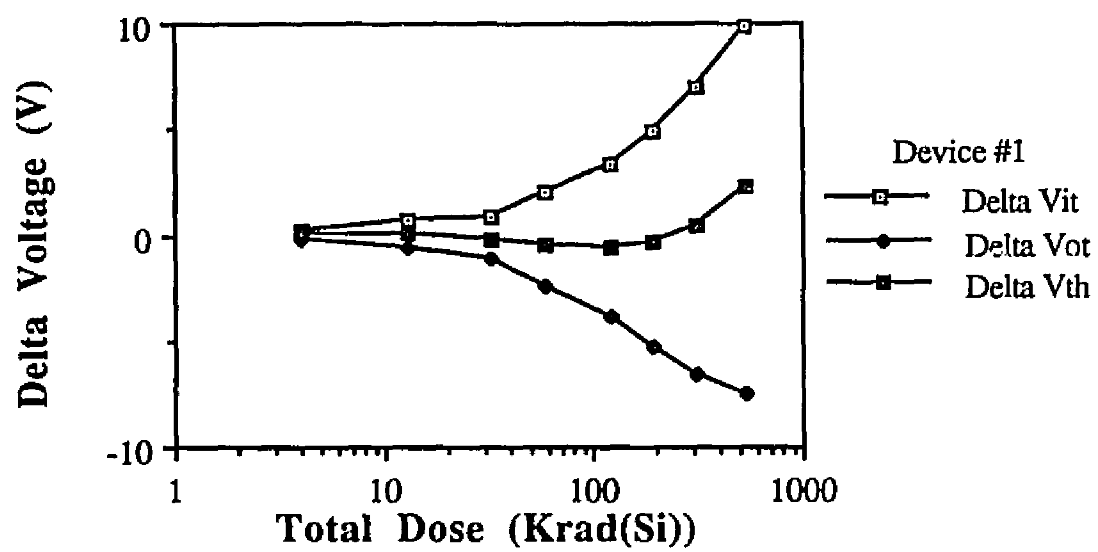

IRH254 Device #1 - Mid-Gap

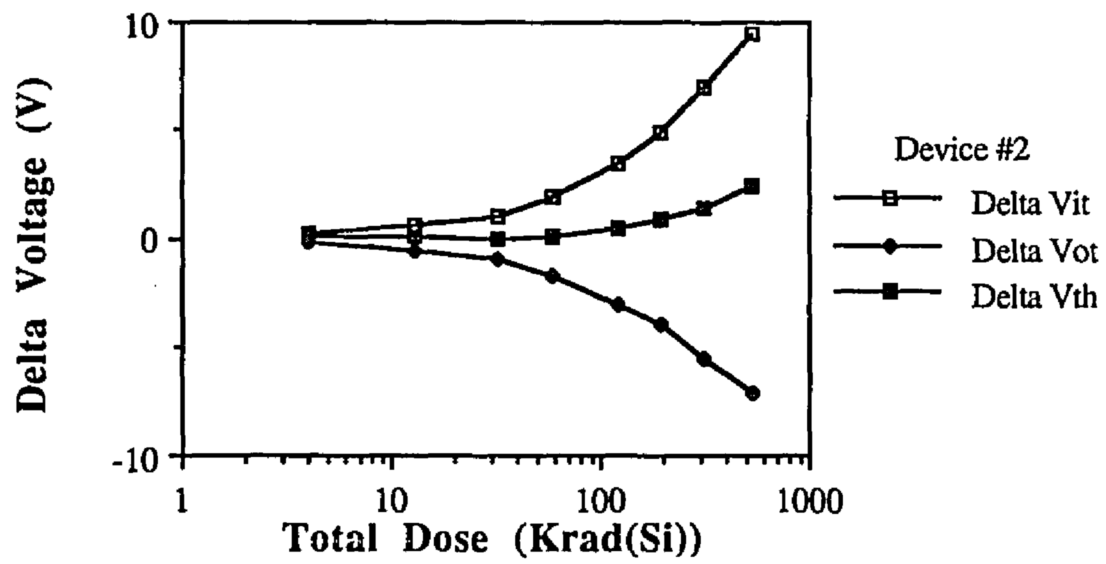

IRH254 Device #2 - Mid-Gap

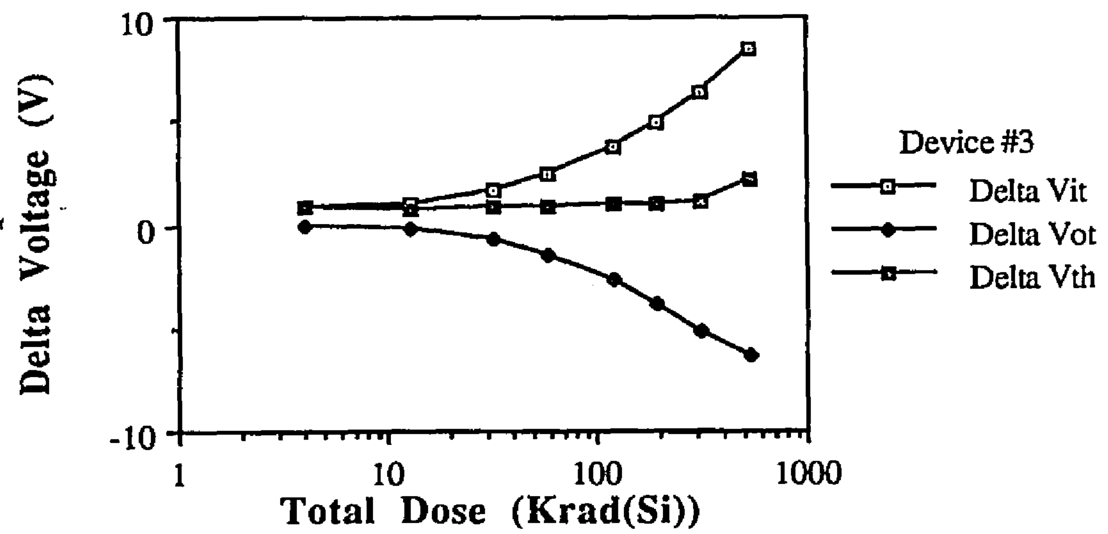

IRH254 Device #3 - Mid-Gap

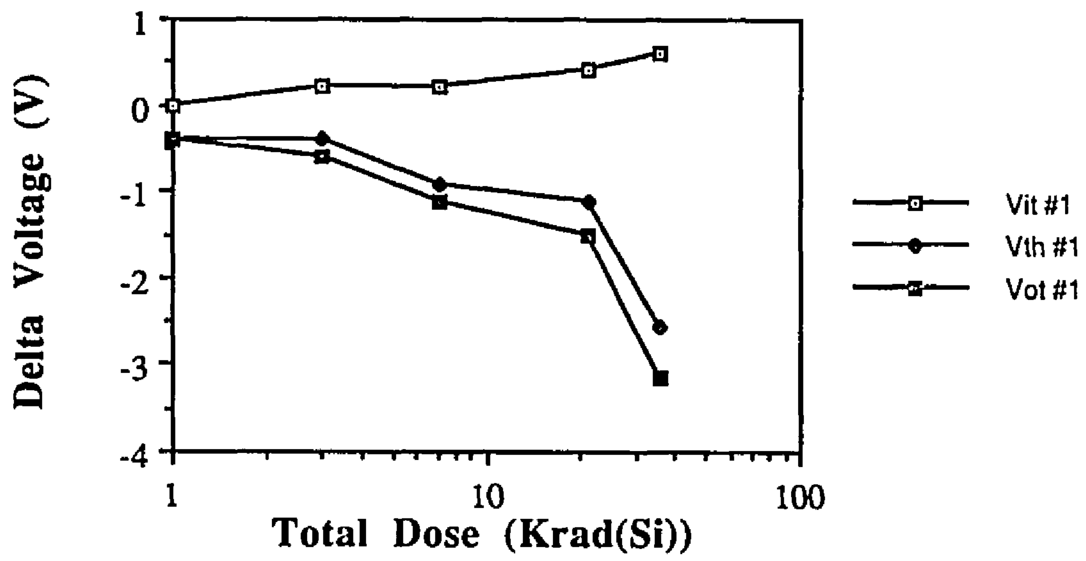

IRF440 Device #1 - Gate-Charge

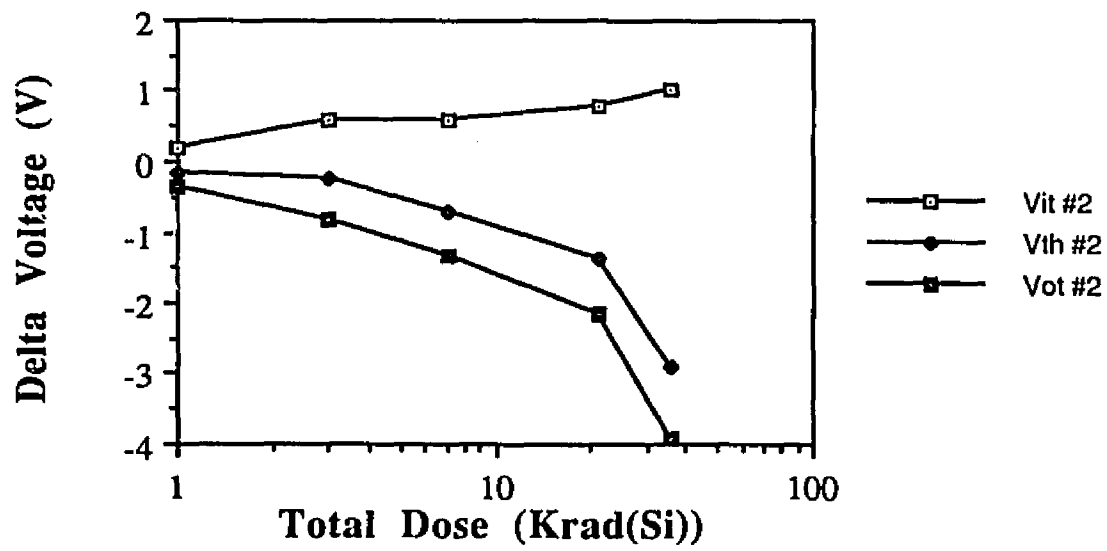

IRF440 Device #2 - Gate-Charge

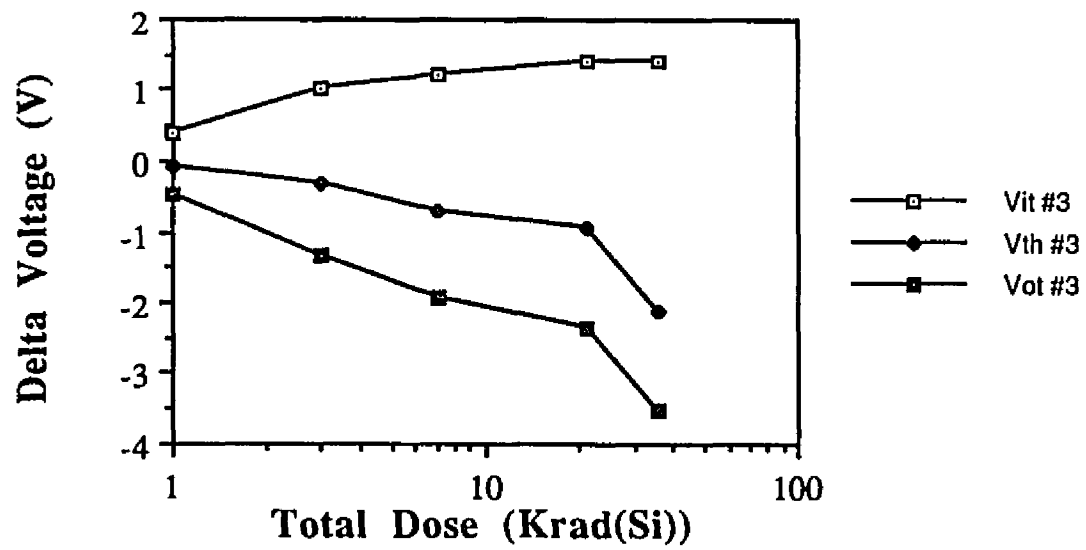

IRF440 Device #3 - Gate-Charge

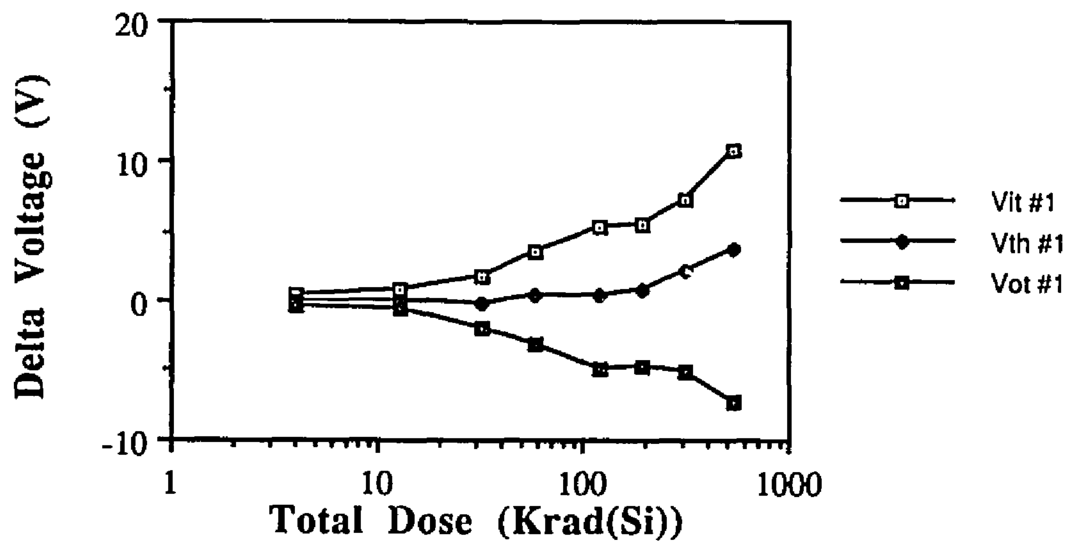

IRH254 Device #1 - Gate-Charge

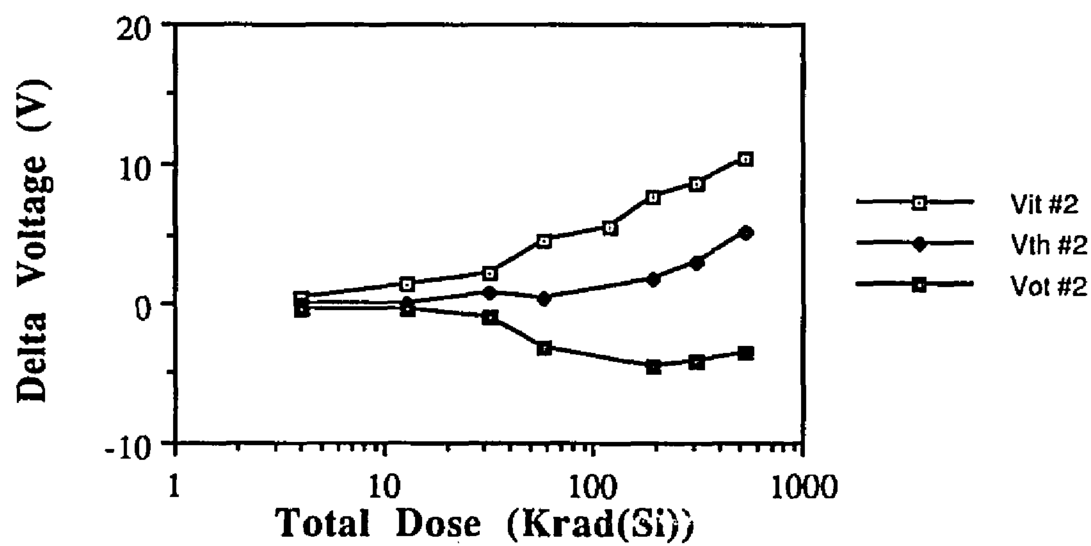

IRH254 Device #2 - Gate-Charge

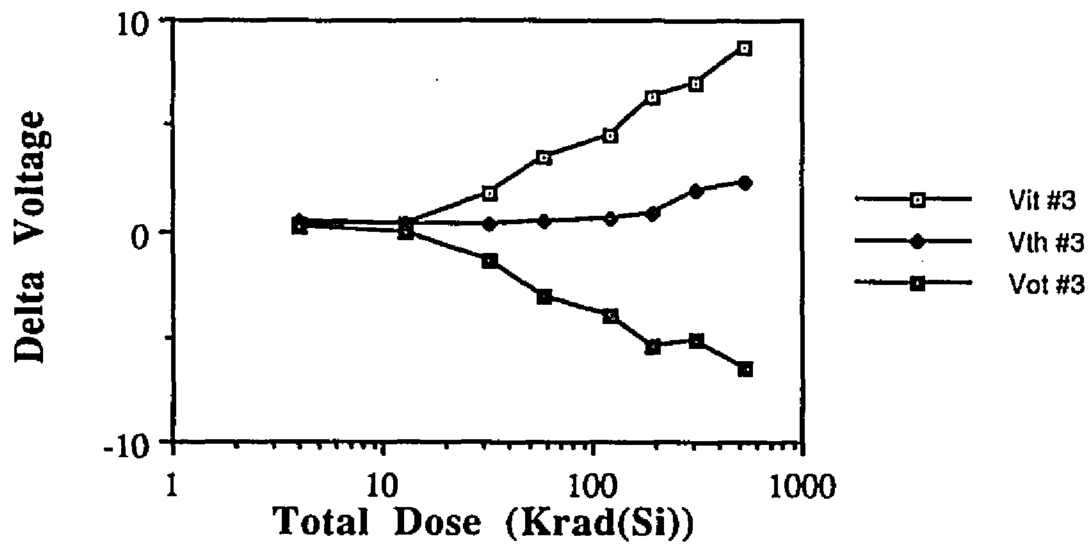

IRH254 Device #3 - Gate-Charge

APPENDIX C
LISTING OF COMPUTER PROGRAM FOR SIMULATION OF MID-GAP METHOD - Written in turbo c by W. Weber

```
#include <stdio.h>
#include <math.h>
char s1[1];
int iplace, istart, istop, irange, iint, itw, it, j, i;
float psf, qn, qnn, nit, v0, psnn, psn, beta5, betap, f1, id, mina, unot, dnuse[200],
ddnit[200], dnit, alpha, a, beta, vg, vf, ps, pss, vgt, dtotal, vvolts, slope, voff, u, charge,
vrange, rt, pms, cox, dv,vmg,gm,flag,vg1,flag1,vg2,inv,vinv,img,
vinp,idm,dvomg,dvtin,dvimg,dvin,dvisw,dvosw,nitsw,nitmg,dslope;
main()
{FILE *fpp, *fopen();
printf("Enter output filename \n");
scanf("%s",s1);
fpp=fopen(s1,"w");
beta=1/.0259;
cox=8.85e-14*3.9/1e-5;
pms=5.1/beta;
mina=1.5e10/1e16;
a=10.0;
dnit=0.0;
alpha=8e-12;
unot=750.0;
vgt=2.0e0;
istop=0;
irange=150;
dtotal=0.0e0;
istart=1;
printf("Enter Flat-Band Voltage \n");
scanf("%f",&vf);
printf("Enter voltage range of Interface Distribution in Energy in eV \n");
scanf("%f",&vvolts);
again:
printf("Divide the interface distribution up into sections of constant slope and enter the
slope and the voltage run for the constant regionv - units slope: # of traps /cm-2/eV voltage
```

```
psf)*(exp(ps)-ps-1))));
ps=ps/beta;
pss=ps-psf/beta+vvolts/2;
itw=pss*150/vvolts;
if(itw<1){itw=1;}
if(itw>150){itw=150;}
u=unot*(1/(1+alpha*dnuse[itw]));
betap=beta*ps;
if(itw<75){nit=1;}
else{nit=-1;}
vg=vg-1.6e-19*dnuse[itw]*nit/cox+vf;
charge=dnuse[itw]*nit;
id=u*8000*a*(cox/(2*(pow(beta,2))))*(pow(rnina,2))*(1-exp(-
beta5))*(exp(betap))*(pow(betap,-.5));
if(flag>0){goto skip;}
if(id>5e-9){vg1=vg; flag=1;}
skip:
if(flag>1){goto idm;}
if(id>5e-8){vg2=vg; flag=2;}
idm:
if(flag1>0){goto idm2;}
if(id>inv){vinp=vg; flag1=1;}
idm2:
fprintf(fpp,"%6.5e %6.5e\n",id,vg);}
betap=psf;
idm=1500*2*a*(cox/(2*(pow(beta,2))))*(pow(rnina,2))*(1-exp(-
beta5))*(exp(betap))*(pow(betap,-.5));
slope=(log10(5e-9)-log10(5e-8))/(vg1-vg2);
dvomg=vg1+(log10(idm)-log10(5e-9))/slope-vmg;
dvtin=vinp-vinv;
dvimg=dvtin-dvomg;
dslope=(log10(5e-9)-log10(5e-8))/(.920-1.11)-slope;
dvisw=psf/log(10)*dslope;
dvosw=dvtin-dvisw;
nitsw=cox*dvisw/1.6e-19;
nitmg=cox*dvimg/1.6e-19;
printf("Dvnit mid gap %5.3e, Dvnit Swing %5.3e, input nit %5.3e \n",nitmg, nitsw,
dnuse[150]);
```

```
end:
printf("%e \n",dnuse[150]);
fclose(fpp);}
```

LIST OF REFERENCES

1. W.E. Baker Jr., "The Effects of Radiation on the Characteristics of Power MOSFETs," *Proc. POWERCON 7*, vol. D3-1-6, 1980.

2. G.C. Messenger and M.S. Ash, *The Effects of Radiation on Electronic Systems*. New York: Van Nostrand-Reinhold, 1986, pp. 222-243.

3. N.S. Saks and D.B. Brown, "Interface Trap Formation via the Two-Stage H^+ Process," *IEEE Trans. Nucl. Sci.*, vol. NS-36, pp. 1848-1857, 1989.

4. F.B. McLean, H.E. Boesch, and T.R. Oldham, "Charge Generation, Transport, and Trapping," in *Ionizing Radiation Effects in MOS Devices and Circuits*, T. P. Ma and P. V. Dressendorfer, Ed., New York, NY: Wiley-Interscience, 1989, pp. 47-51.

5. P.J. McWhorter and P.S. Winokur, "Simple Technique for Separating the Effects of Interface Traps and Trapped-Oxide Charge in Metal-Oxide-Semiconductor Transistors," *Appl. Phys. Lett.*, vol. 48, p. 133, 1986.

6. D.A. Grant and J. Gowar, *Power MOSFETs Theory and Applications*. New York: Wiley, 1989, pp. 15-31.

7. H. Hughes, "Historical Perspective," in *Ionizing Radiation Effects in MOS Devices and Circuits*, T. P. Ma and P. V. Dressendorfer, Ed., New York, NY: Wiley-Interscience, 1989, pp. 47-51.

8. G.A. Ausman and F.B. Mclean, "Electron-Hole Pair Creation Energy," *J. Appl. Phys.* **45** p. 4506, 1974.

9. H. Hughes, "Historical Perspective," in *Ionizing Radiation Effects in MOS Devices and Circuits*, T. P. Ma and P. V. Dressendorfer, Ed., New York, NY: Wiley-Interscience, 1989, pp. 149-167.

10. Peter S. Winokur, "Radiation-Induced Interface Traps," in *Ionizing Radiation Effects in MOS Devices and Circuits*, T.P. Ma and P.V. Dressendorfer, Ed., New York, NY: Wiley-Interscience, 1989, p. 178.

11. Peter S. Winokur, "Radiation-Induced Interface Traps," in *Ionizing Radiation Effects in MOS Devices and Circuits*, T.P. Ma and P.V. Dressendorfer, Ed., New York, NY: Wiley-Interscience, 1989, pp. 169-170.

12. G. Groeseneken, H.E. Maes, M. Beltran, and R.F. DeKeersmaecker, "A Reliable Approach to Charge-Pumping Measurements in MOS Transistors," *IEEE Trans. Electron Devices*, vol. ED-31, p. 42, 1984.

13. S.M. Sze, *Physics of Semiconductor Devices*. New York: Wiley-Interscience, 1981, p. 482.

14. K. Gauen, "Gate Charge and Input Capacitance – Complementary Specifications of MOSFET Input Impedance," *Powertechnics*, July, 1986.

15. S.M. Sze, *Physics of Semiconductor Devices*. New York: Wiley-InterScience, 1981, pp. 442-443.

16. J.R. Brews, "Subthreshold Behavior of Uniformly and Nonuniformly Doped Long-Channel MOSFET," *IEEE Trans. on Electron Devices*, vol. ED-26, p. 1282, 1979.

17. S.M. Sze, *Physics of Semiconductor Devices*. New York: Wiley-Interscience, 1981, p. 77.

18. K.F. Galloway, M. Gaitan, and T.J. Russell, "A Simple Model for Separating Interface and Oxide Charge Effects in MOS Device Characteristics," *IEEE Trans. Nucl. Sci.*, vol. NS-31, pp. 1497-1501, 1984.

19. R.F. Pierret, *Field Effect Devices*, Modular Series on Solid-State Devices Vol. IV, R.F. Pierret and G.W. Neudeck, Eds., Reading, Mass: Adison-Wesley, 1983, pp. 31-38.

20. R.D. Schrimpf, K.F. Galloway, and P.J. Wahle, "Interface and Oxide Charge Effects on DMOS Channel Mobility," *Electronics Lett.*, vol. 25, pp. 1156-1158, 1989.

21. P. Grey and R. Meyer, *Analog Intragrated Circuits*. New York: Wiley & Sons, 1984, pp. 68-71.